GULF GENERAL ATOMIC

Gulf-GA-A12421

GAS-COOLED FAST BREEDER REACTOR

QUARTERLY PROGRESS REPORT

FOR THE PERIOD AUGUST 1, 1972 THROUGH OCTOBER 31, 1972

by

Project Staff

Prepared for the
U.S. Atomic Energy Commission
San Francisco Operations Office
Under
Contract AT(04-3)-167
Project Agreement No. 23

Gulf General Atomic Project 393

December 8, 1972

GULF GENERAL ATOMIC COMPANY
P.O. BOX 608, SAN DIEGO, CALIFORNIA 92112

PROGRESS REPORT SERIES

GA-5537	November 1, 1963 to July 31, 1964
GA-6667	August 1, 1964 to July 31, 1965
GA-7645	August 1, 1965 to July 31, 1966
GA-8107	August 1, 1966 to July 31, 1967
GA-8787	August 1, 1967 to July 31, 1968
GA-8895	August 1, 1968 through October 31, 1968
GA-9229	November 1, 1968 through January 31, 1969
GA-9359	February 1, 1969 through April 30, 1969
GA-9639	May 1, 1969 through July 31, 1969
GA-9811	August 1, 1969 through October 31, 1969
GA-9838	November 1, 1969 through January 31, 1970
GA-10517	February 1, 1970 through January 31, 1971
GA-10645	February 1, 1971 through April 30, 1971
GA-A10803	May 1, 1971 through July 31, 1971
GA-A10906	August 1, 1971 through October 31, 1971
GA-A12003	November 1, 1971 through January 31, 1972
GA-A12165	February 1, 1972 through April 30, 1972
GA-A12252	May 1, 1972 through July 31, 1972

ABSTRACT

The tasks of the Gas-Cooled Fast Breeder Reactor (GCFR) program supported by the U.S. Atomic Energy Commission are program planning, core development, development of pressure equalization system for fuel rods, fuels and materials development, and nuclear analysis and reactor physics. Core development work included structural and thermal analyses of the fuel-element assembly, studies of the effects of fuel hot-pressing with burnup on fuel temperature, development of an analytical model for the monitor station instrumentation for the pressure equalization system, and further criticality studies of the lower shield assembly. Work on the planning document for the pressure equalization system for the fuel rods was initiated. In fuels and materials development, the status of the thermal-flux and fast-flux irradiation programs are given. The results of postirradiation examinations to date of the GB-9 fuel rod irradiated in the thermal flux of the ORR and of the G-3 fuel rod irradiated in the EBR-II fast flux are given. Reactor physics studies included critical assembly analysis, in particular, calculations of small-sample worths, Doppler worth, β_{eff}, and prompt lifetime, and the conversion to ENDF/B Version III for GCFR calculations.

CONTENTS

Figures

Tables

1. INTRODUCTION

The Gas-Cooled Fast Breeder Reactor (GCFR) program sponsored by the U.S. Atomic Energy Commission consists of five tasks: Task 1000—Program Planning, Task 4100—Core Development, Task 4160—Pressure Equalization System for Fuel, Task 4200/4400—Fuels and Materials Development, and Task 4700—Nuclear Analysis and Reactor Physics. The broad objectives of each of these tasks and a summary of the work done on each task during the period covered by this report are given in this section. The work performed under each task during the period is presented in Sections 2 through 6.

The GCFR Utility Program, which is supported by a large number of electric utility companies, rural electric cooperatives, and Gulf General Atomic, is primarily directed toward the development of a 300-MW(e) GCFR demonstration plant. This utility-sponsored work and the AEC-sponsored work are complementary.

1.1. TASK 1000—PROGRAM PLANNING

Work on this task is directed toward detailing plans for the technical development of the GCFR concept. The development program planning document that has been prepared identifies and defines the developmental items necessary for supporting the design, construction, and operation of a 300-MW(e) GCFR plant. The document contains the analytical and test programs required and the schedules and estimated costs for the development tasks. Since the beginning of fiscal year 1972, essentially all of this work has been privately supported.

Draft copies of the three volumes of the Development Program Plan for the 300-MW(e) GCFR plant have been submitted to the Atomic Energy Commission.

In addition, this task provides for liaison with Argonne National Laboratory (ANL) and Oak Ridge National Laboratory (ORNL) on tasks they are performing under AEC funding; the corresponding work at Gulf General Atomic is being privately funded.

1.2. TASK 4100—CORE DEVELOPMENT

The objective of this task is the engineering development of the reactor core and associated components. The various investigations carried out under this task during this reporting period are given in Section 3.

Analytical studies of the fuel-element assembly are directed toward developing the design criteria for selecting a fuel-rod spacer reference design. Improvements have been made in formalizing the factors influencing fuel-element distortions that could affect the rod-spacer design. Applicable computer codes are being modified and developed for calculating thermal-hydraulic conditions in the fuel element and for fuel-element and fuel-rod bowing. In the development of analytical methods for predicting fuel rod behavior, the effects of fuel hot-pressing were studied.

In the analytical studies of the monitor station instrumentation for the pressure equalization system, modification and further development of a computer program was initiated.

Evaluation studies of the lower shield assembly design included further criticality investigations to assess potential secondary criticality from the melting of a few fuel elements.

1.3. TASK 4160—PRESSURE EQUALIZATION SYSTEM FOR FUEL

The objective of this task is to develop a system for equalizing the pressure between the inside and the outside of the GCFR fuel rod. A separate development planning document is to be prepared for the pressure equalization system for the GCFR.

Work on the planning document has been initiated, an outline has been prepared, and a format is being established that will comply with applicable RDT standards.

1.4. TASK 4200/4400—FUELS AND MATERIALS DEVELOPMENT

The fuels and materials development and testing program extends and applies Liquid-metal Fast Breeder Reactor (LMFBR) fuel technology to GCFR requirements. This includes surveillance of the LMFBR fuels and materials

program to utilize existing and developing technology applicable to the GCFR and to determine areas where GCFR work complements the development of LMFBR fuel technology. The status of the thermal-flux and fast-flux irradiation test programs is presented in Section 4.

In the postirradiation examination (PIE) of the GB-9 fuel rod, an electron microprobe analysis was made of a transverse metallographic sample of the GB-9 fuel to determine radial burnup distribution and optical metallography was performed at five axial positions along the fuel rod to determine fuel behavior and cladding attack.

Irradiation of the vented fuel rod GB-10 was started August 29, 1972, and by October 31, 1972, a burnup of 4,200 MWd/Te had been reached. Initial operation of the rod is at a linear heat generation rate of 12 kW/ft and will continue at this rate to approximately 10,000 to 15,000 MWd/Te.

The fast-flux irradiation experiment F-1 (X094A) reached a burnup of ~44,000 MWd/Te in EBR-II.

Postirradiation examination of the G-3 rod removed from the F-1 experiment is continuing at ANL.

The five replacement fuel-rod capsules for the F-1 (X094A) experiment have been shipped from ORNL to EBR-II and the data package containing the "as fabricated" details of the capsules is currently being prepared.

Design changes were made in the capsule for the fuel rods to be irradiated in the F-3 fast-flux irradiation experiment to facilitate fabrication and handling of both the GGA and ANL capsules.

1.5. TASK 4700—NUCLEAR ANALYSIS AND REACTOR PHYSICS

This task involves the surveillance of LMFBR physics work and critical experiments to properly coordinate and develop a complementary GCFR nuclear analysis and physics program. The work performed under this task during this reporting period is discussed in Section 6.

Efforts continued on surveillance of LMFBR critical assembly experiments with the objective of establishing an experimentally verified basis for GCFR reactor physics work. Emphasis was placed on calculation of small-sample

central worths in the voided inner core of ZPPR-2. Application of two-dimensional transport theory to correct for flux depression in r-z perturbation calculations showed significant improvement in the agreement between measured and calculated worths. Conversion of GGA data files to ENDF/B Version III was completed. Liaison with ANL continued, both through the Industrial Participation Program and through direct contact with members of the ANL staff.

2. TASK 1000—PROGRAM PLANNING

Draft copies of the three volumes of the Development Program Plan for the 300-MW(e) Gas-Cooled Fast Breeder Reactor plant have been submitted to the Atomic Energy Commission.

In order to have intermediate comparative checks between the SAS computer program being modified at ANL to include a gaseous coolant and the equivalent programs that have been developed at GGA under private funding, two separate sample problems were sent to ANL. The information transmitted included a description of the fuel-rod geometry, the material properties used, and the results of two flow-reduction cases where the reactor flow was reduced from 100% to 50% linearly over a 30-sec period. The first case assumed a constant 100% reactor power (no control-rod motion or reactivity feedbacks) and the second case assumed no control-rod motion but with Doppler, axial expansion, and coolant density feedbacks. Detailed fuel-rod temperature maps at various times during the transient were sent for the two cases.

3. TASK 4100—CORE DEVELOPMENT

3.1. FUEL-ELEMENT ASSEMBLY

Analytical work on the fuel-element assembly has continued toward the goal of developing the design criteria necessary for selection of a fuel-rod spacer reference design concept. During this reporting period there has been an improved formalization of the factors influencing fuel-element distortions that could affect the spacer design. These factors are categorized below and their interactions are shown schematically in Fig. 3.1.

Operating Conditions:

1. Normal operation
   a. Neutron flux and spectrum,
   b. Power (temperature),
   c. Time,
   d. Gradients of flux and power;
2. Off-design operation (transient conditions);
3. Operational procedures, such as rotation of the fuel elements at each refueling period.

Design Features:

1. Rod-to-rod pitch and the allowable tolerance;
2. Clearance between the spacer support and the fuel rod;
3. Thermal-hydraulic design of fuel rod and spacer;
4. Spacing from edge of rod to fuel-element box wall;
5. Axial spacer-grid separation.

Fabrication Features:

1. Initial rod bow;
2. Offset of spacer grids;

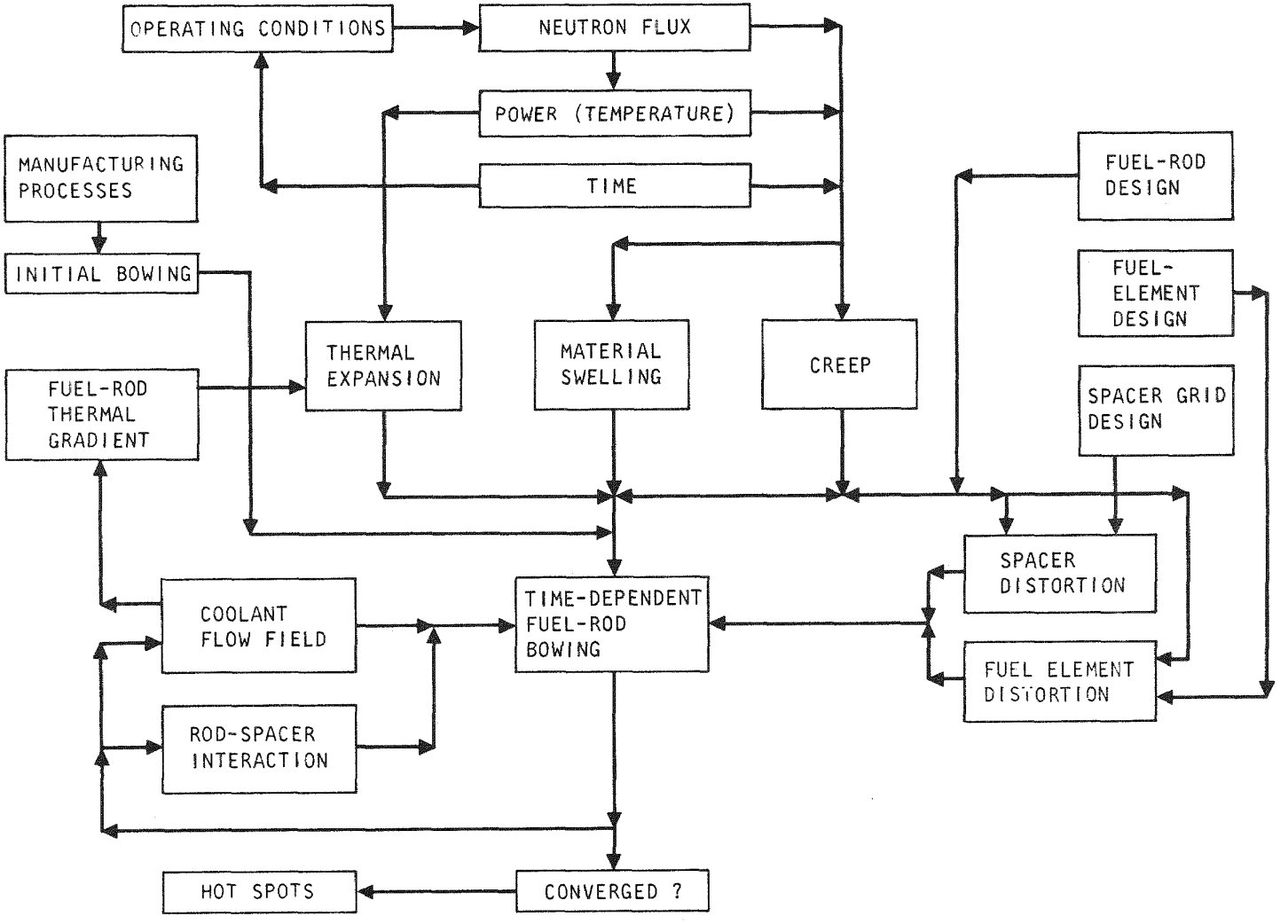

Fig. 3.1 Schematic representation of factors influencing fuel-rod bowing

3. Actual spacer cell-to-cell spacing.

These factors establish an initial set of thermal-hydraulic conditions at the beginning of rod life that determine the detailed flow and temperature distributions in the fuel-element assembly. In turn, the temperature and flux distributions cause time-dependent deformations of the fuel rods, the spacer grids, and the fuel-element box. These deformations modify the temperature distribution within the assembly and thereby change the course of subsequent time-dependent distortions.

The objective is to maintain the fuel-rod hot spots below the reference condition of 700°C throughout the life of the fuel element. The analytical approach to this problem is based on the interrelated effects discussed above and uses an iterative method, i.e., the initial thermal conditions within the fuel assembly are determined, the time-dependent distortions resulting from the factors operating on this initial condition are calculated, and after some time step, the thermal distribution that results from these distortions is recalculated. This process will then be reiterated until a picture of what is happening over the lifetime of the fuel element is obtained.

The initial calculations are based on steady-state operations. Transient conditions and forces resulting from fuel-rod vibrations have not yet been included in the calculations. Earlier calculations have shown that rod bowing is the limiting criterion for establishing the positions of the spacers and that hydraulically induced rod vibrations will not be important under these conditions. These conclusions will be verified later in the program after a specific spacer design has been selected for further analysis and flow testing.

In the early stages of these calculations, the focus has been on development of analytical tools, analysis of nominal design conditions, and parametric and sensitivity studies of conditions varying from the nominal design. The progress made in these analyses is discussed below in Section 3.1.1, Structural Analysis, and in Section 3.1.2, Thermal Analysis.

One of the considerations in the structural analysis is the axial force imposed on the spacers by interaction with the fuel rods due to

differential thermal expansion during power changes. This interaction will depend on the coefficient of friction between the rod and the spacer under reactor operating conditions in a helium coolant. Experimental work is being initiated to yield this information, as discussed in Section 3.1.3.

3.1.1. Structural Analysis

3.1.1.1. Rod Bowing. The analyses of rod and fuel-element bowing were made using the creep analysis of statistically indeterminate beams code, CRASIB,[1] which is a two-dimensional structural analysis code using finite-element techniques and includes the time-dependent effects of irradiation swelling and thermal- and irradiation-enhanced creep.

The creep behavior is obtained in the code by using an iterative approach, and a wide range of creep laws may be used. The beam may be made up of 10 different materials, have 10 different cross sections, and be supported at as many as 100 points. The beam environment may include 100 concentrated load points, linear temperature gradients, and a linear flux gradient, which, coupled with the linear temperature gradients, results in nonlinear swelling.

The analytical results produced as output for the beam at hot operating conditions are

1. A centerline displacement profile,
2. The reaction forces at each beam support, and
3. Stress and strain (total and creep) radial profiles at each node point,
4. Final output is all of the above data after the beam is cooled.

Two subroutines are being developed for inclusion in the CRASIB code to determine the effect of fuel-element rotation. These are described as follows:

Subroutine Rotate. This changes the temperature and power (flux) level and reverses the temperature and neutron flux gradients. The rotation is inherently limited to 180°.

Subroutine Stuff. This is a modified version of the CRASIB subroutine STIFF, and its purpose is to change the temperature-dependent values of the elastic modulus and thermal expansion coefficient used in the

calculations after element rotation to compensate for the power-level change. The stiffness matrix generated by the subroutine STIFF is not changed from the beginning-of-life value.

The GCFR fuel rod has an outside diameter of 0.285 in. and the cladding wall thickness is 0.019 in. The fuel rod is held firmly at the upper fuel-rod support grid, and in the current design, eight spacer grids are equally spaced 9.1 in. along the rod. The fuel rod is held at its lower end by the bottom guide and spacer grid. The fuel rod is constrained from axial motion at the upper fuel-rod support grid but is allowed to move freely in the axial direction at all other supports. At the bottom fuel-rod support, the axial motion of the fuel rod relative to the element box is restricted to less than 0.75 in. (nominal). A schematic of the fuel rod and spacer arrangement is shown in Fig. 3.2 and the axial node arrangement used is shown in Fig. 3.3. The 36 nodes used were arranged to indicate spacer locations, general fuel-rod distortion, beginning of active core, start of rod roughening, end of active core, and upper and lower rod support grids.

The axial temperature profiles used in the calculations are shown in Fig. 3.4. The temperatures of the fuel rod or cladding and of the fuel-element box were taken to be the same in the upper blanket region (602°F). In the lower blanket region, the cladding temperature was 1147°F, whereas the fuel-element box temperature was 1100°F. In the core region, the box temperature distribution was assumed to be linear between 602°F and 1100°F.

The axial profile of the radial temperature gradient in the lower blanket region of the rod was approximated. The detailed nature of the temperature field in a GCFR fuel element was established with the HETHRA code (discussed in Section 3.1.2). For the fuel-element box calculations, the radial temperature gradient of the rod was input, as described above, with the gradient dropping to zero at the end of the fuel rod. Two radial temperature gradients were used in calculations of the fuel rod. The lower radial temperature gradient was identical to that used for the fuel-element box. The higher radial temperature gradient of the rod had a linearly dependent nature from 0.0°F/in. at the top of the active core to 80°F/in. at the bottom of the active core and then down to 20°F/in. at the bottom of the lower blanket region, as shown in Fig. 3.5.

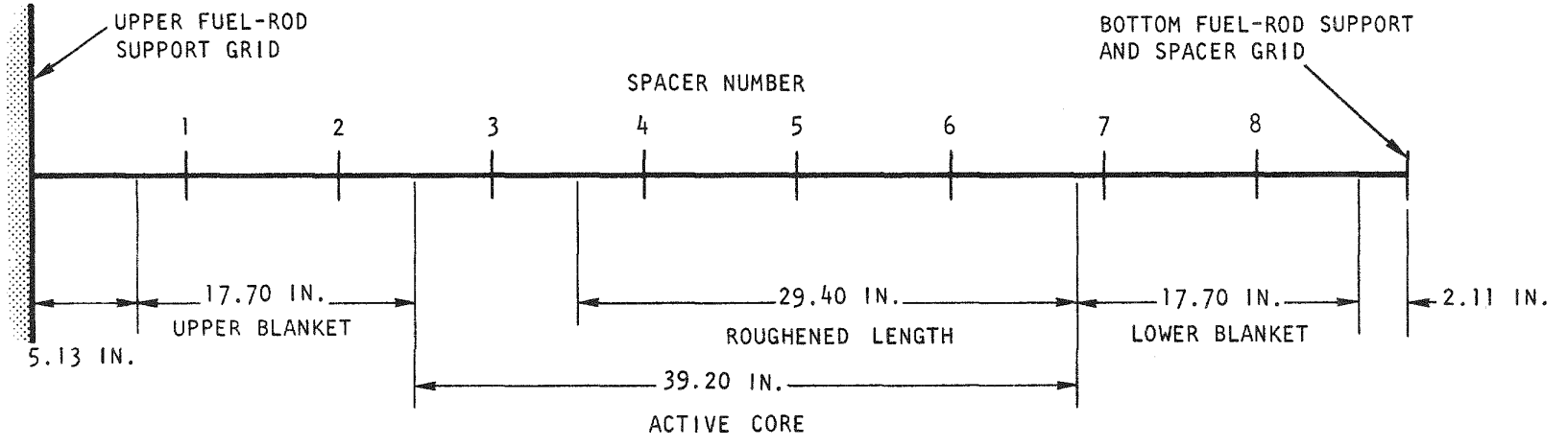

NOTES:

8 SPACER GRIDS EQUALLY SEPARATED 9.1 IN. ALONG ROD

FUEL ROD 0.285 IN. DIAM., 0.019 IN.-THICK CLADDING WALL.

Fig. 3.2 Schematic of GCFR fuel rod and spacer arrangement

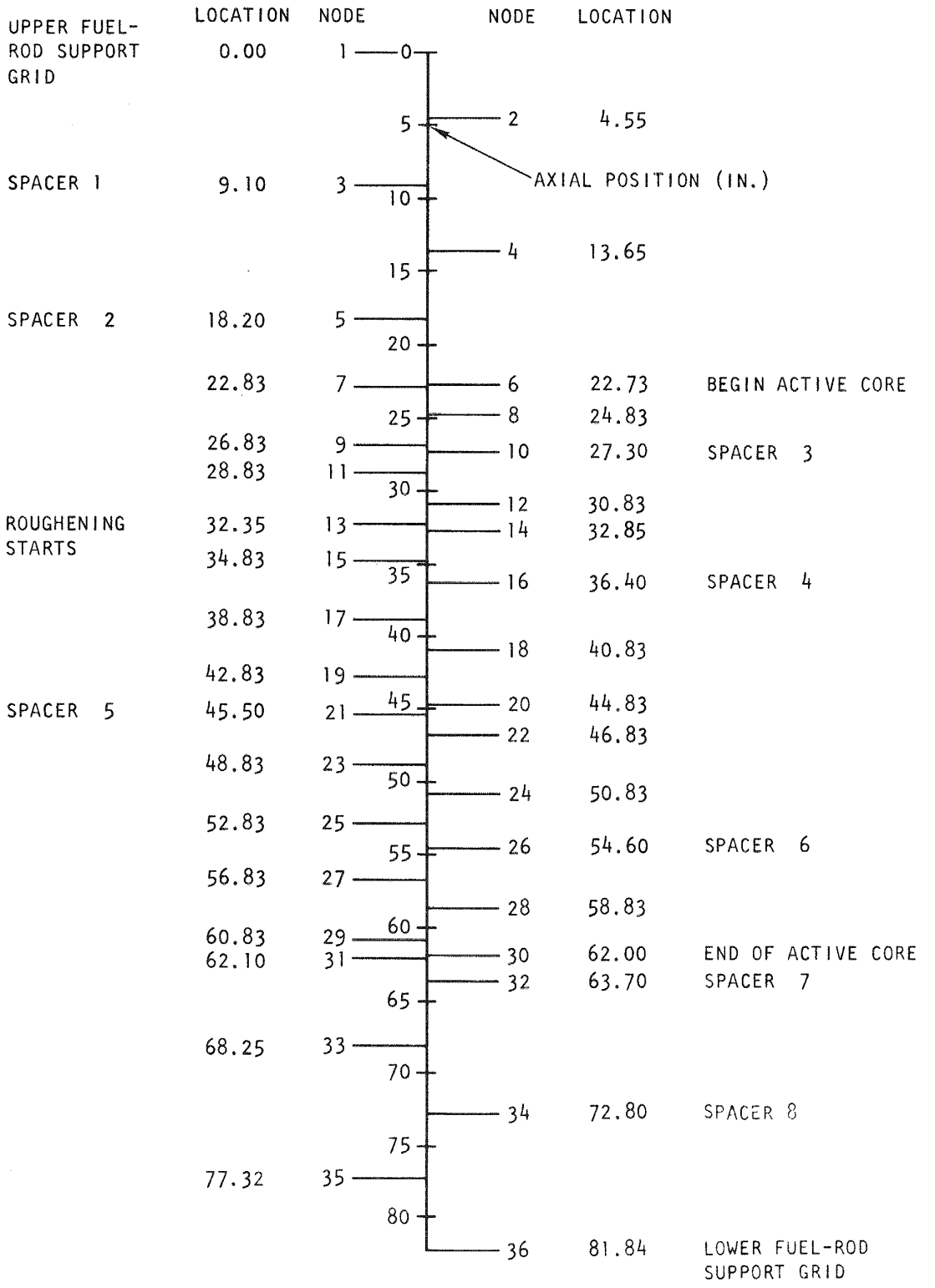

Fig. 3.3 Nodal arrangement for fuel-rod bowing study

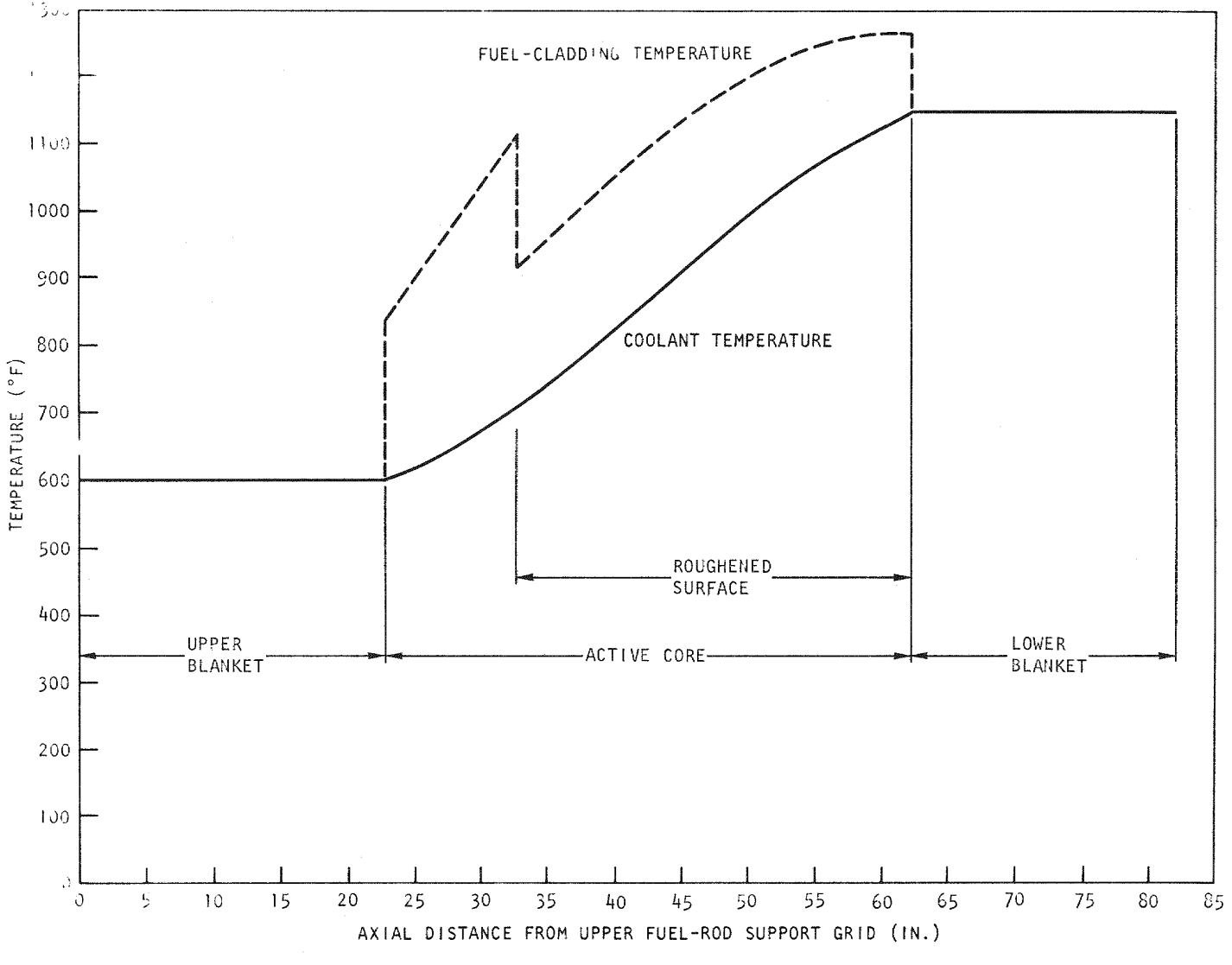

Fig. 3.4 Axial distribution of coolant and fuel-cladding temperature

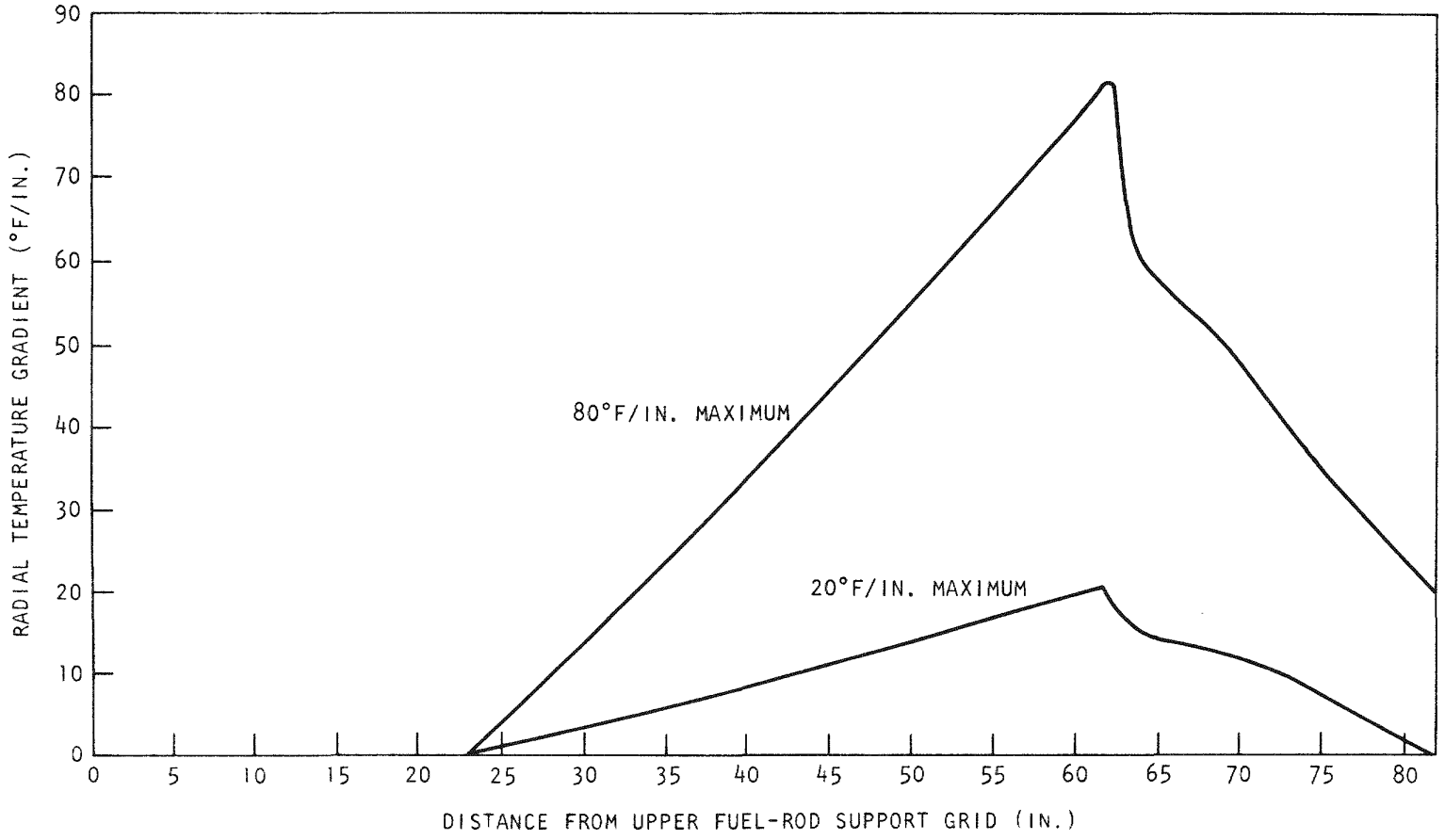

Fig. 3.5 Radial temperature gradients for fuel rod used in fuel-element box calculations

The axial neutron flux profile used in all of the calculations is shown in Fig. 3.6; the profile was intended to be sinusoidal with a maximum core center value of 3.44×10^{15} neutrons/cm^2/sec. The flux is used in the material growth correlation and is for energies greater than 0.1 MeV. The radial flux gradient was taken as 5.6%/in.

The temperature-dependent values of Young's modulus and the thermal expansion coefficient used in the CRASIB code were calculated from correlations given in Ref. 2:

$$E \pm 2\sigma = 2.944 \times 10^{7} - 6.374 \times 10^{3}\ T,$$

where E = Young's modulus (psi),
T = temperature (°F),
$2\sigma = 1.242 \times 10^{6}$ (psi),

and

$$\alpha \pm 2\sigma = (8.555 + 1.499 \times 10^{-3}\ T) \times 10^{-6}$$

where α = coefficient of linear thermal expansion (in./in./°F),
T = temperature (°F),
$2\sigma = 0.498 \times 10^{-6}$ (in./in./°F).

The volumetric swelling correlation and the creep correlation, including temperature- and radiation-induced creep, are Eqs. (28) and (29) from the LIFE-II code.[3]

The first consideration in the analysis of rod bowing was to select the most severe situation among the fuel rods in the reactor. This was taken to be the highest-powered rod of a fuel element at the core-radial blanket interface. Further, because the thermal-hydraulic feedback is believed to be most significant for fuel rods at the outside corners of the hexagonal rod array, i.e., at the corner coolant flow subchannels, a fuel element with its corner toward the core centerline was selected for the analysis. Therefore, the bowing investigation was based on the inside corner rod in this type of fuel element.

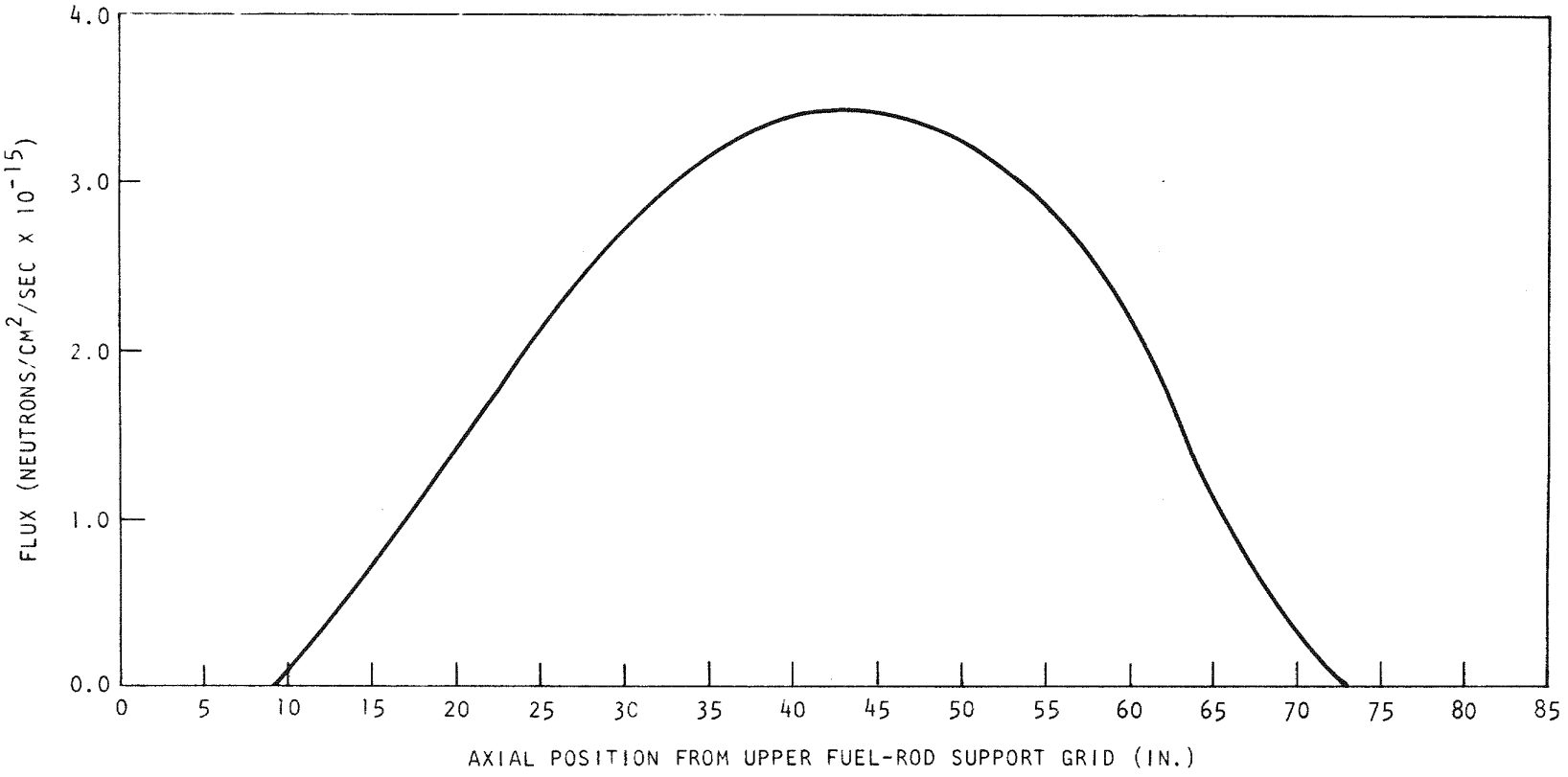

Fig. 3.6 Axial neutron-flux profile used for fuel-rod bowing calculations

Analyses of a rod in this "worst" position were then conducted to investigate the cases summarized in Table 3.1. The results for each case analyzed are given below.

Case 1: As shown in Fig. 3.7, the maximum displacement of 0.005 in. occurs at 20,000 FPH for the GCFR reference design of eight equally spaced grids with a maximum radial temperature gradient of 20°F/in. For all cases examined, the maximum displacement occurs at the design life of 20,000 FPH and is not linear with time. It may also be noted that in all cases in which eight equally spaced grids were used, the maximum displacement is near the outlet end of the active core.

Case 2: The results for this case are shown in Fig. 3.8; they are similar to those shown in Fig. 3.7 for case 1 except that the maximum displacement was 0.014 in. and all displacements are about a factor of 3 greater than those of case 1. This is due to the increase in the radial temperature gradient from 20°F/in. to 80°F/in. The maximum displacement occurred at the same axial position—namely, the bottom end of the core.

Cases 3 and 4: To assess the effect of spacer misalignment, four spacers were offset 0.007 in. for case 3 and the same spacers were offset 0.012 in. for case 4. The shape of the displacement versus axial position curve for case 4 is shown in Fig. 3.9. Again, the maximum displacement is at 58 in. and in this case has a maximum value of 0.009 in. compared to the reference design (case 1) in which a maximum displacement of 0.005 in. was used. In case 3, where the offset was smaller (0.007 in.), the maximum displacement was also proportionately smaller.

Case 5: In this case, spacers 3, 4, and 6 were removed to gain insight into how the rod would bow if the number of restraints were reduced. The analysis was made with no element rotation, with the 20°F/in. maximum radial temperature gradient, and with the rod held at the 0.0 in. radial position at the spacers. The bowing calculated is shown in Fig. 3.10. The bowing at 20,000 FPH goes from 0.048 in. at 32 in. to 0.036 in. at 54 in. This is compared to a maximum bow of 0.005 in. for case 1, the reference case.

Case 6: To determine the fuel-rod bowing relative to the fuel-element box as influenced by bowing of the hexagonal box was the purpose of case 6.

Table 3.1

CASES INVESTIGATED IN THE GCFR ROD BOWING STUDY

Case No.	Purposes	Structure	Number of Spacer Grids	Fuel Element Rotation	Maximum Radial Temp. Gradient	Comments
1	(a) Reference design, (b) Effect of operating lifetime	Fuel rod	8	None	20°F/in.	Rod held at 0.0 in. at all spacers (see Fig. 3.7).
2	Effect of radial temperature gradient	Fuel rod	8	None	80°F/in.	Rod held at 0.0 in. at all spacers (see Fig. 3.8).
3	Effect of misalignment of spacers	Fuel rod	8	None	20°F/in.	Rod held at 0.007 in. radial displacement at spacers 1, 4, 5, 8.
4	Effect of misalignment of spacers	Fuel rod	8	None	20°F/in.	Rod held at 0.012 in. radial deflection at spacers 1, 4, 5, 8 (see Fig. 3.9).
5	Influence of losing restraint at several spacers	Fuel rod	5	None	20°F/in.	Rod held at 0.0 in. radial displacement at spacers, with spacers 3, 4, and 6 removed (see Fig. 3.10).
6	Effect of fuel-element box distortion on rod bowing	Fuel rod	8	None	20°F/in.	Rod held at 450 FPD fuel-element radial distortion.
7	Effect of an additional spacer at critical location	Fuel rod	9	None	80°F/in.	Rod held at 0.0 in. radial displacement at all spacers (see Fig. 3.12).

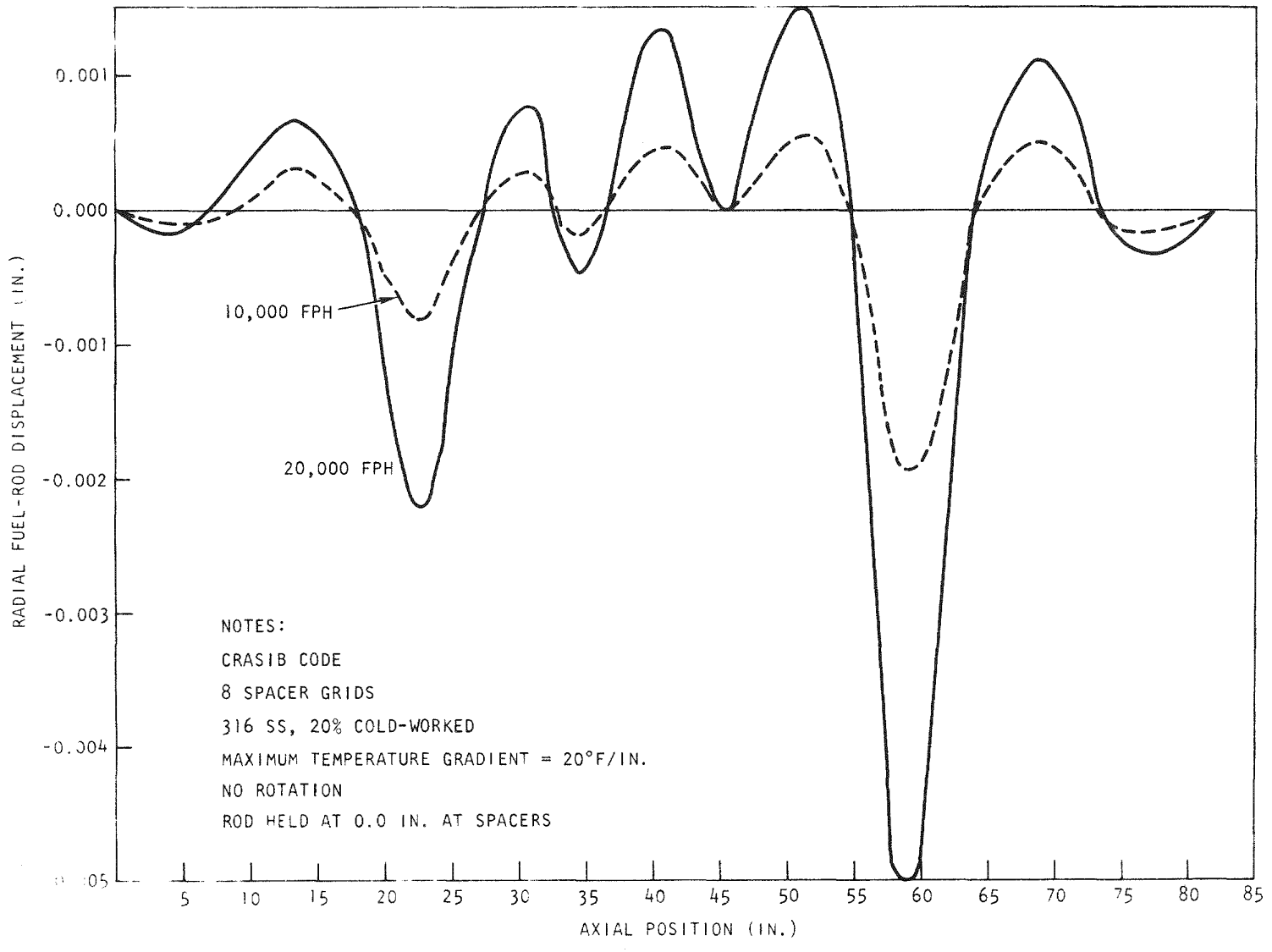

Fig. 3.7 Fuel-rod bowing vs. axial position - Case 1

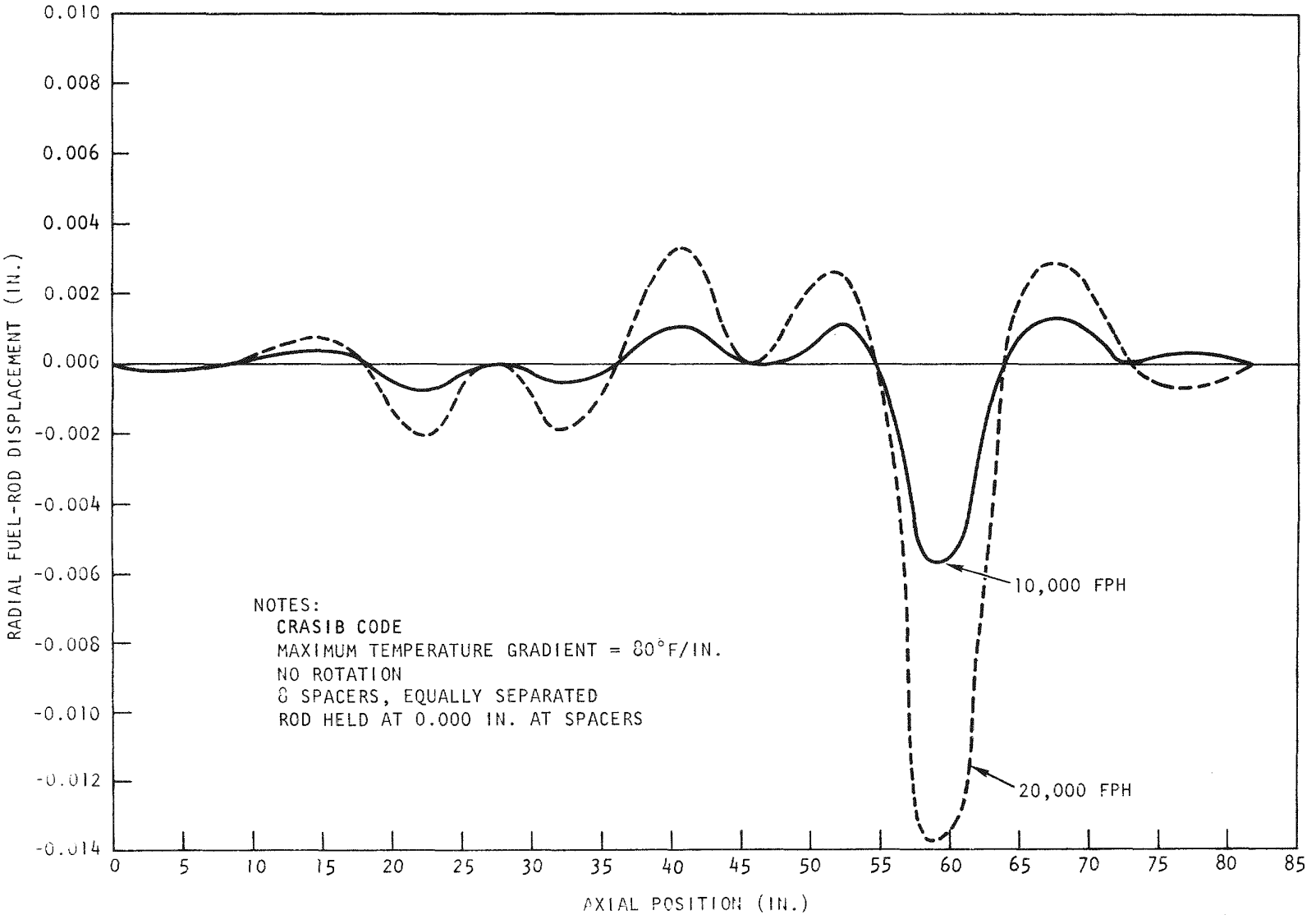

Fig. 3.8 Fuel-rod bowing vs. axial position - Case 2

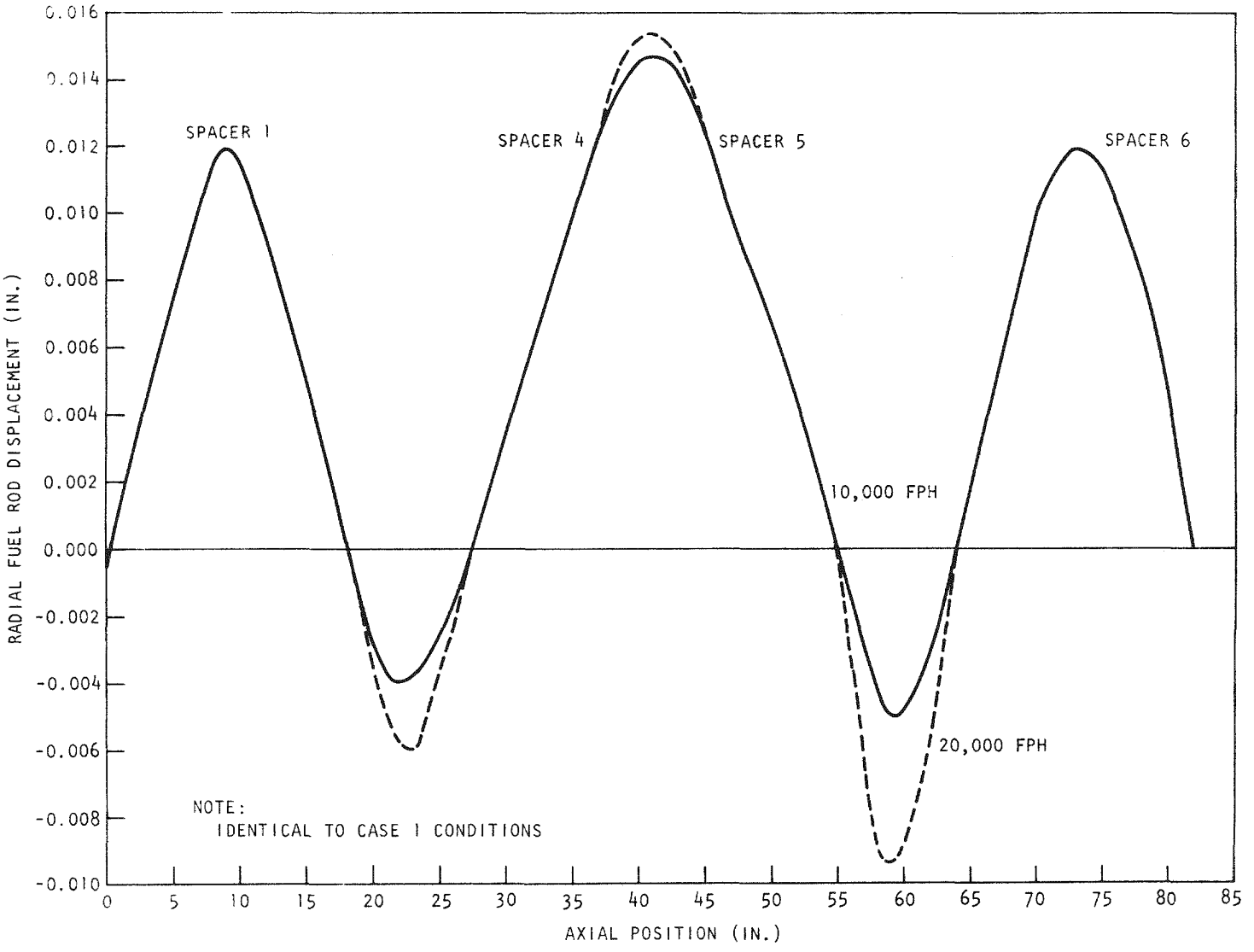

Fig. 3.9 Fuel-rod bowing vs. axial position with spacers 1, 4, 5, and 6 displaced 0.012 in. from center - Case 4

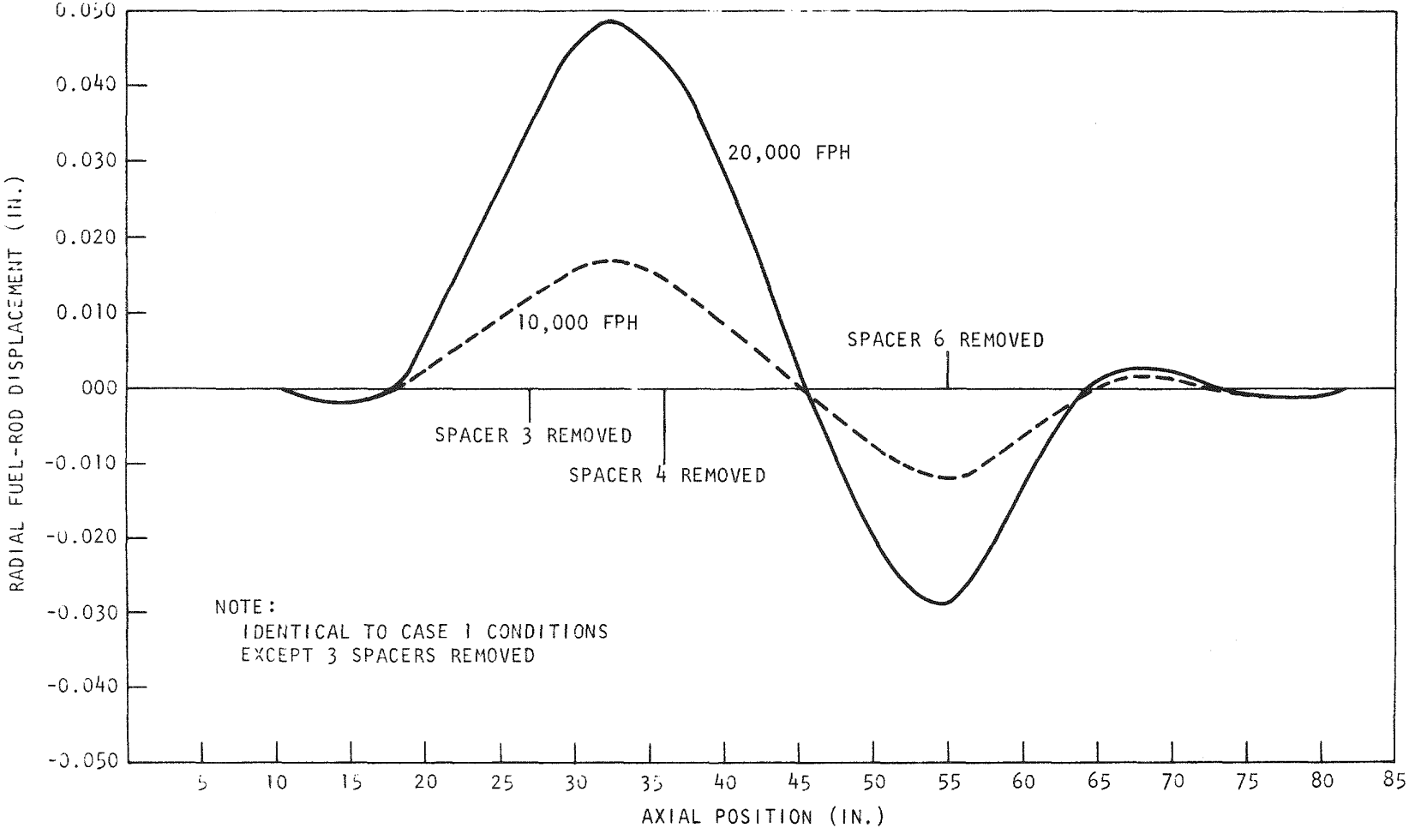

Fig. 3.10 Fuel-rod bowing at 10,000 FPH and 20,000 FPH vs. axial position with spacers 3, 4, and 6 removed - Case 5

investigation of these elastic properties has been conducted using the experimental data from a previous grid bending test (described in Ref. 4) in which a spacer grid was subjected to a point central axial loading and central deflections were measured as a function of load value. These were compared with Horvay's model,[5] which reduces the perforated spacer grid to a solid flat plate with effective elastic properties, namely, E^* and ν^*. The equations developed by Horvay are:

$$E^* = AE\, h/R \tag{3.1}$$

and

$$\nu^* = 1 - \frac{4}{3 + 2(1 + \nu)n + L^2/4h^2} \tag{3.2}$$

where $A = 1 - \nu^*$,

E = Young's modulus for 316 SS at room temperature,

h = half-thickness of grid ligaments,

R = (grid pitch)/2,

ν = Poisson ratio (0.3),

n = 1.2 (see Ref. 5),

L = length of one side of grid cell.

The dimensions of the test grid were:

$h = 0.005$ in.

$R = 0.115$ in.

$L = 0.248$ in.

Using the test grid dimensions and $E = 29 \times 10^7$ psi, the values determined were $E^* = 4380$ psi and $\nu^* = 0.9985$ from Eqs. (3.1) and (3.2). These are the analytical values that must agree with the experimental results if the test grid can be represented by Horvay's effective plate model.

Next, the experimentally determined values of load, W, and deflection, δ, were used to calculate the E^* necessary to satisfy the condition that the grid can be treated as a flat-plate model. This was done by using the plate bending formulas from Roark[6] for simply supported edges and for clamped edges. These formulas are as follows:

The fuel-element hexagonal box was subjected to flux gradients similar to the fuel rod and to temperature gradients of the coolant flowing within. Since the box is much stiffer than the 271-rod array contained in it, the rod bundle conforms to any bowing of the hexagonal box. Fuel-element distortions after 450 FPD in core zone 4 (at the core-blanket interface) with no rotation are shown in Fig. 3.11. With the rod conforming to the 450-FPD assembly distortion, and with a 20°F/in. maximum radial temperature gradient, with 8 spacers, and with no fuel-element rotation, case 6 was run to 20,000 FPH. The relative rod-bowing results were essentially the same as those for identical conditions without fuel-element bowing, i.e., case 1.

These results are encouraging since it appears to establish that the rod bowing relative to the element box bowing is independent of element bowing.

Case 7: Because the worst deflections were always experienced at the same location, a ninth spacer was added and the rod was held at 0.0 in. radial displacement, with other conditions similar to the previous cases. The addition of one spacer had a significant influence on the bowing calculated, as can be seen in Fig. 3.12. The maximum bowing (at 20,000 FPH) changed from 14 mils at 59 in. in case 2 to 4.6 mils at 41 in. in case 7. The rod bowing at 41 in. at 20,000 FPH was 3.6 mils in case 3; for case 7 there was an increase of 1 mil at 41 in. but a decrease of about 10 mils of maximum displacement due to the added spacer.

Case 7 gives good evidence that marked reductions in radial rod deflections or fuel-rod bowing can be achieved if a nonuniform spacer grid separation scheme is used. Specifically, the spacers should be closer together in the active core region and separated farther in the axial blankets. This will be discussed in more detail later.

3.1.1.2. Spacer-grid Bending Correlation. The axial forces acting on the fuel rods will tend to amplify the fuel-rod bowing. These axial forces mainly result from friction between the fuel rod and the spacer grid during differential thermal expansion and swelling growth. The magnitude of the forces are proportional to the elastic bending properties of the grid. An

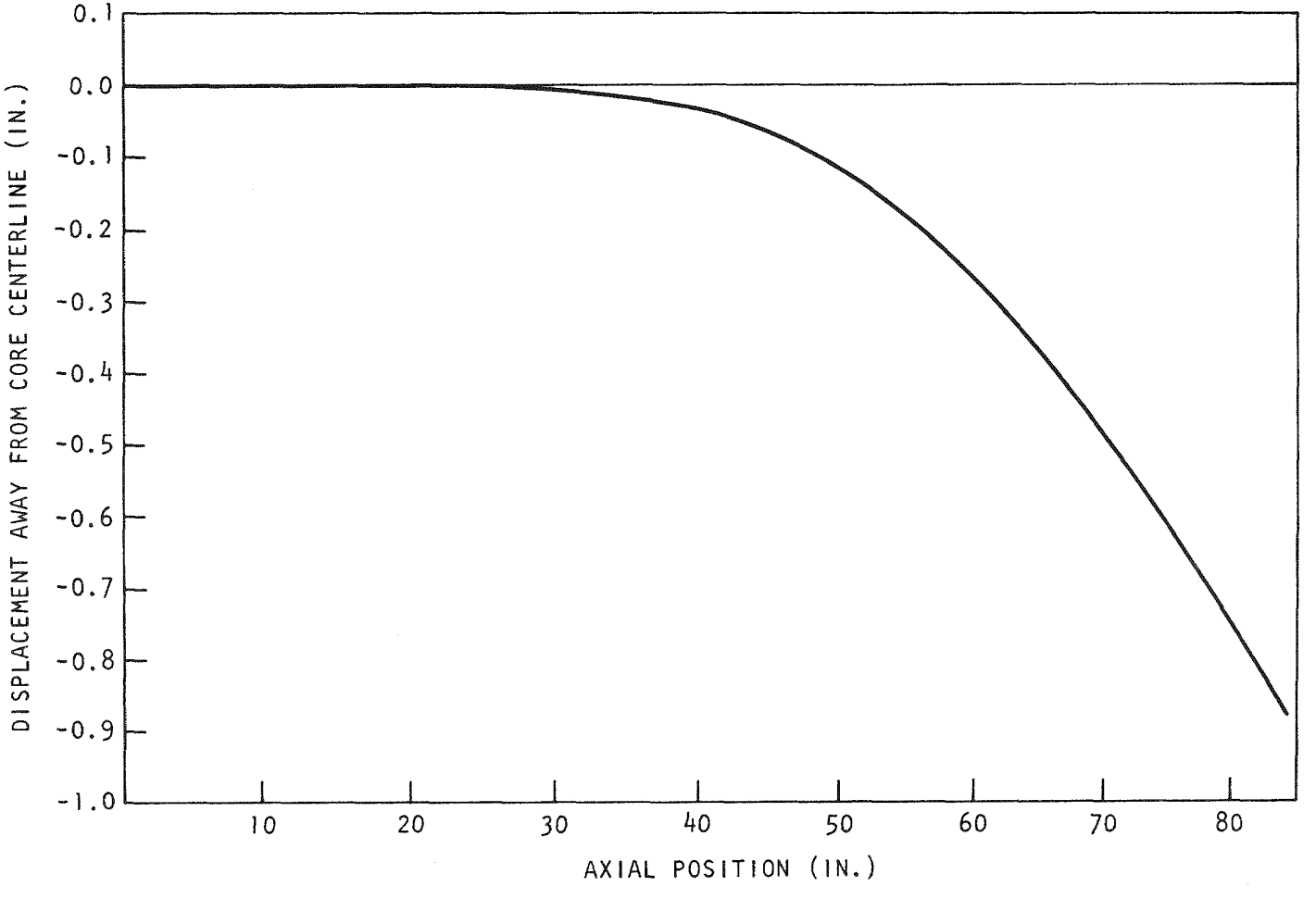

Fig. 3.11 Distortion of fuel element at 450 FPD with no rotation - Case 6

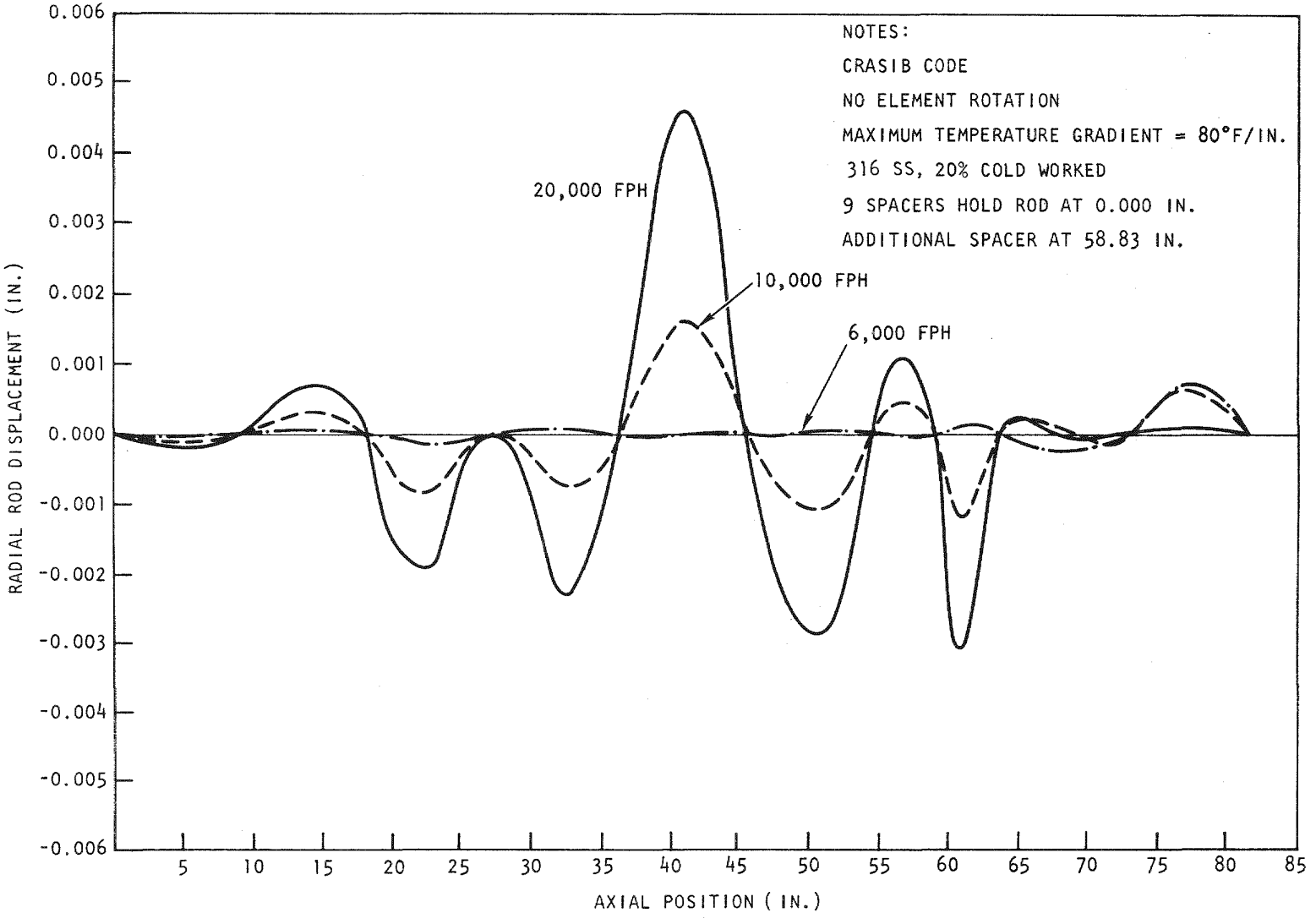

Fig. 3.12 Fuel-rod bowing vs. axial position for nine spacers using linear growth correlation - Case 7

Simply Supported Edges

$$E^* = \frac{W}{\delta_{max}} \frac{3(m - 1)(3m + 1)R_{eq}^2}{4\pi m^2 t^3} \tag{3.3}$$

Clamped Edges

$$E^* = \frac{W}{\delta_{max}} \frac{3(m^2 - 1)R_{eq}^2}{4\pi m^2 t^3}, \tag{3.4}$$

where W = central load,

δ_{max} = central deflection,

m = reciprocal of ν^*,

R_{eq} = equivalent radius of grid,

t = depth of grid in axial direction.

Using the test values for the deflections, δ_{max}, as a function of central load, W, the values of E* were calculated for both cases. One of the unknowns was the value of Poisson's ratio. The value used was $\nu = 0.9985$, as determined from Horvay's model. The results are plotted in Fig. 3.13. A comparison shows that the experimental values of E* calculated with the flat-plate theory are a factor of two to four smaller than the value of E* calculated with Horvay's model. This indicates that the manufactured grids are far more flexible than a grid machined from a solid plate. This is probably because of the spot-welding between grid ligaments, which greatly reduces the ligament efficiency in transmitting central loads to the outer grid structure. That is, the value of ν^* determined from Eq. (3.2) is probably not correct and another correlation should be developed. Also, a distributed load test might show better correlation between experiment and the theory of Horvay's model.

3.1.1.3. Summary of Structural Analysis. The preliminary structural analysis of the GCFR fuel-element assembly discussed above indicates the following conclusions:

1. The bowing of the fuel-element box is markedly reduced by fuel-element rotation.

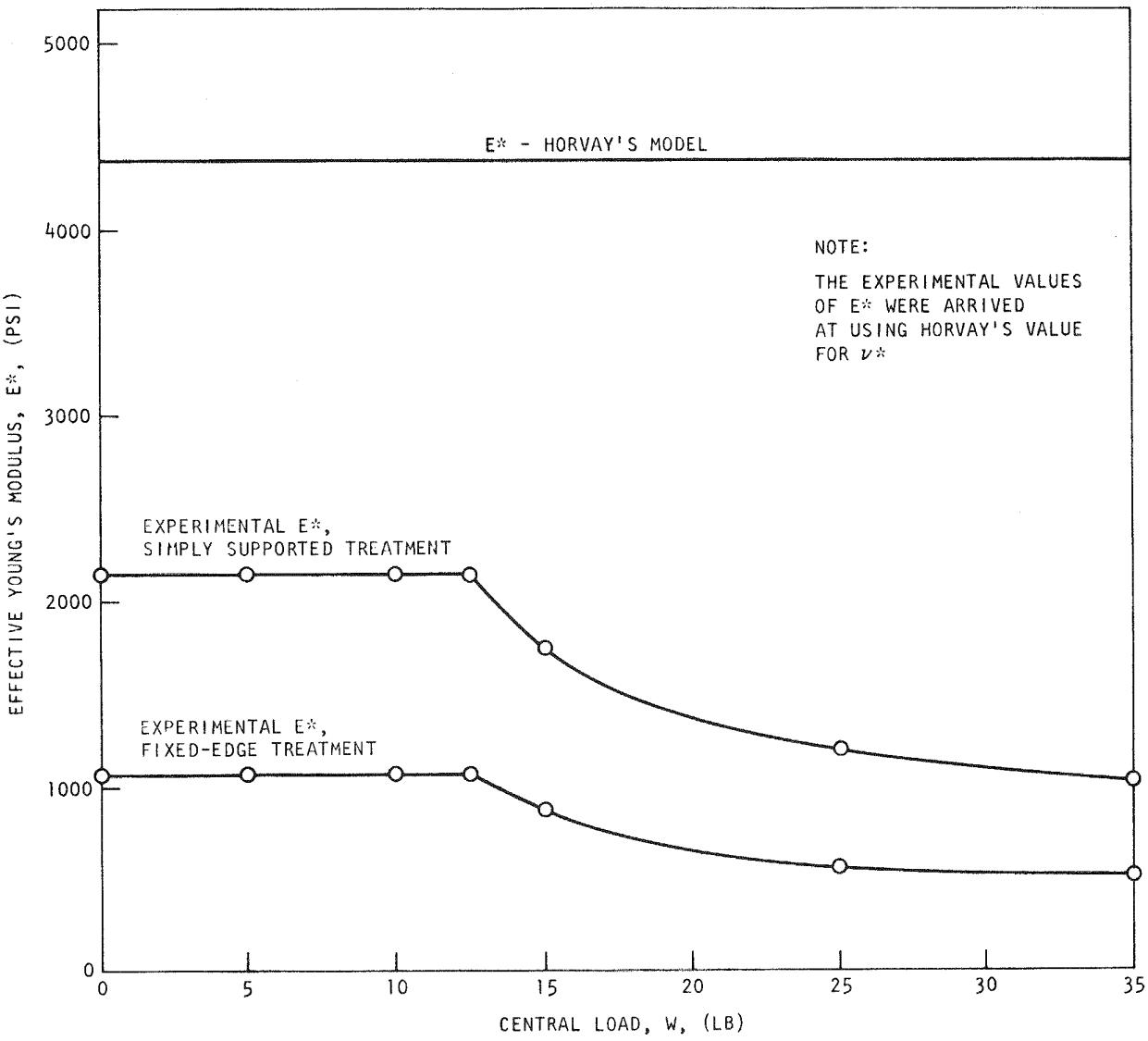

Fig. 3.13 Comparison of experimental and analytical effective Young's modulus, E*

2. An element design with a nonuniform axial separation distance of the spacer grids can be used to reduce the bowing of the fuel rods.

3. The magnitude of fuel-rod radial distortion is not influenced greatly by initial rod distortion caused by spacer radial misalignment.

4. The influence of fuel-element bowing on the relative distortions between the fuel rod and the hexagonal box appears to be quite small.

5. The hexagonal honeycomb grid structure is several times more flexible in axial bending than the hexagonal grid-plate model of Horvay.[5]

Additional work is required in the following areas:

1. Incorporation of real properties of the spacer in the analysis rather than a fixed-node concept,

2. Analysis of the effect of the attachment of the grid spacer to fuel element wall.

3. Analysis of the influence of fuel-element rotation on rod bowing.

4. Extension of the investigation of the role of axial forces.

5. Enlargement of the parametric and sensitivity analysis.

6. Determination of distortion with initial clearance between rod and spacer.

3.1.2. Thermal Analysis

Detailed thermal-hydraulic analysis of the GCFR fuel element is being initiated as part of the overall analysis of fuel-rod distortion and resultant hot spots. The COBRA-II computer program[7] developed for the thermal-hydraulic subchannel analysis of a rod-bundle nuclear fuel element is being modified to determine the detailed performance of the GCFR fuel element with various degrees of distortion. The helium thermal-hydraulic rod-bundle analysis (HETHRA) is the modified version of COBRA-II.

The existing COBRA-II provides for 36 subchannels, 25 fuel rods, and 60 subchannel connections; these numbers are set by the computer storage

limits and the way the storage is used. A GCFR fuel element contains 271 rods, approximately 600 subchannels, and approximately 800 subchannel connections. To apply COBRA-II to the GCFR fuel element, either only a portion of an element will be analyzed or the code storage will have to be changed.

A computation was made of a one-twelfth sector of a GCFR element with nominal geometry and a radial power ratio gradient of 1.05/in. using the HETHRA code. For this sector, the maximum-to-average coolant temperature rise was 1.085 and the temperature-rise ratio gradient was 1.06 per inch. This preliminary result indicates that the effect of power gradient is magnified about 20% in the temperature rise gradient. The maximum inside surface temperature was 1162°F, compared with a nominal reactor average maximum of 1100°F without hot-spot factors and 1292°F with hot spot factors. A turbulent mixing factor of 4 was used in the calculations, as discussed below.

The one-twelfth sector model has many fluid-to-fluid boundaries, and it must be assumed that equal conditions exist on both sides of the boundary. Since distortion at or near the boundary would upset this condition to an unknown degree, an analysis has been started of a small element that is completely enclosed by the element walls so that asymmetric distortion can be treated without the assumption of symmetry. The simplest configuration of interest is a seven-rod bundle, which is the configuration being used in the analysis.

The seven-rod bundle has a high portion of nonheated element wall surface to heated rod surface in comparison to those of larger rod bundles; therefore, the importance of turbulent mixing is emphasized in the seven-rod configuration. Turbulent mixing between subchannels is the chief means of exchanging heat between subchannels and reducing temperature peaks. The effect of the turbulent mixing factor, Y, on coolant temperature rise and the temperature difference between wall and coolant is shown in Table 3.2. For comparison, the results for an infinite lattice (no box wall effects) case are included. A review of the literature on turbulent mixing in rod bundles indicates a mixing factor of Y = 3 to 5 using the formulation of Ingesson.[8] Ingesson presents a correlation for the GCFR bundle configuration that yields a value of Y = 5 for smooth-surface rods. Experimental

Table 3.2

EFFECT OF TURBULENT MIXING PARAMETER ON SEVEN-ROD BUNDLE WITH UNIFORM HEATING

Subchannel Type		Coolant Temperature Rise (°F)	Heat-transfer Temperature Difference (°F)	Maximum Cladding Temperature—Inlet Temperature (°F)
Infinite lattice		417	164	581
Seven-rod bundle				
Center subchannel	Y[a] = 5	433	199	632
	= 4	436	198	634
	= 3	441	198	638
	= 2	447	198	645
	= 1.25	456	197	653
	= 0	495	199	694
Wall subchannel	Y = 5	406	205	611
	= 4	405	207	612
	= 3	402	209	611
	= 2	394	206	600
	= 1.25	381	200	582
	= 0	308	186	493
Wall corner subchannel	Y = 5	410	209	619
	= 4	408	207	615
	= 3	406	205	611
	= 2	408	209	617
	= 1.25	416	218	634
	= 0	502	244	747

[a]Y = turbulent mixing parameter.

Infinite Lattice

T_{in} = 590°F

Rod OD = 0.285

Pitch = 0.389 in.

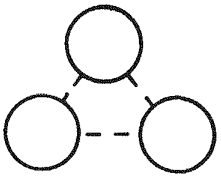

Seven-rod Bundle

$T_{out\ (avg)}$ = 1007°F

Rod-to-wall distance = 0.04 in.

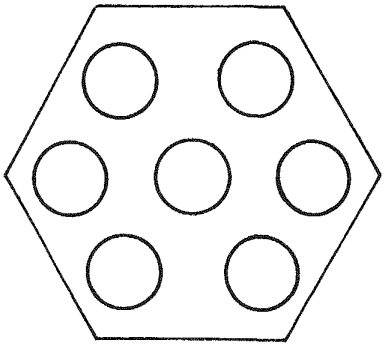

values in the range of Y = 2.5 to 7 are reported in the literature. The sensitivity of the calculations to the turbulent mixing factor does not seem to be very great, based on the results of Table 3.2.

The HETHRA code now appears developed to the point where it might be used in conjunction with CRASIB to analyze fuel-rod distortions iteratively, as described above.

3.1.3. Fuel-rod–Spacer Interaction Tests

In the GCFR fuel-element reference design, the grid spacers are supported from the walls of the fuel-element box. Because of the thermal expansion difference between the fuel rods and the fuel-element box, changes in reactor power will result in relative motion of the rods and spacers. Depending on the clearance between the rod and the spacer and the coefficient of friction associated with the helium environment, this motion will result in frictional forces that either cause deformation of the spacer grid or subject the support mountings to stress cycling. Deformation and misalignment of the rods and grid spacers will affect the frictional forces. The clearance between the rod and spacer will vary over the core lifetime to an extent that is not known exactly. There will be wear that will increase the clearance between the surfaces, but for certain temperature regions, creep and irradiation-induced swelling of the fuel-rod cladding and spacer materials will tend to reduce this clearance.

To obtain design guide values for the frictional forces and wear to be expected under the reactor thermal operating conditions, tests will be conducted on pairs of rod and spacer specimens.

Specifically, the goals of the tests are (1) to quantitatively evaluate the frictional force between single rods and representative spacer sections as a function of spacer design, the interaction force between rod and spacer, the helium purity, temperature, and duration of test and (2) to qualitatively evaluate the problems of wear and fretting as a function of the same variables. These tests are initially to be scoping in nature and thus will not be made under simulated operating conditions; rather, they will provide input as to what ranges of helium impurities and force are allowable for reactor operation. A secondary goal is to determine the

degree and type of corrosion that might occur in a helium environment by measuring changes in weight and by metallographically examining test sections contained in the test environment.

Based on these goals, the following set of test criteria were established.

1. All tests will be conducted on single rods, but the design of all test facilities will take into consideration the eventual extension of testing to rod bundles.

2. Mass flow rates of helium similar to those anticipated in the reactor are not required; the only requirement for mass flow is to ensure that (a) sufficient reactants are present and (b) the reactions are not limited by mass transport in the gas phase.

3. Initial testing of gas purity effects will be conducted over wide ranges of helium impurity levels to determine whether (a) there is a critical impurity level below which there is a significant increase in friction and associated problems and (b) there are critical impurity levels at higher ranges beyond which the mechanism of film formation drastically changes. Analyses will have to be provided to define the gas mixture and impurity levels required to accomplish this goal.

4. Axial motion will be provided by mechanical cycling. The cycling train will be instrumented to provide data on loads versus number of cycles.

5. Interaction forces between the rod and the spacer will be provided by transverse spring-loading of either the rod or spacer and will cover a range of values, including those anticipated from the spacer analysis (see Section 3.1.1).

6. Although the length of the axial stroke is a variable, under reactor operating conditions it is essentially fixed by differential thermal expansion and therefore may be treated as a fixed quantity in this study.

7. Even though the initial results may indicate the need for wear-resistant coatings, it is not anticipated that these will be included in the early phases of the test program.

8. The temperature range studied will be varied over the range from the reactor inlet temperature to slightly above the maximum anticipated cladding temperature (700°C).

A test program meeting these criteria has been established. The testing will be performed by moving a sample of fuel-rod cladding back and forth through a single cell of the fuel-element spacer. The stroke lengths used will be representative of the maximum motion expected for small and large power changes in the reactor. The test duration has been set at 100 hr, allowing one test per week per test station to be performed. The tests will be intermittent, which will allow surface films to reform between strokes, as would occur in reactor operation. Strokes of 1-in. and 0.1-in. have been selected with rates of 1 and 40 per hour, respectively. The temperature range covered will be 325°C to 750°C. Transverse loading will cover the range of 0.5 to 3 lb, in agreement with calculated interaction forces.

The test atmosphere will be helium with various amounts of H_2 and H_2O. The test pressure has been set at 2 atm absolute, which will require concentrations of H_2 and H_2O to be 43 times that at reactor operating pressure of 85 atm to maintain the same partial pressures. Water levels to be used will correspond to values of 0.01 to 1 ppm at 85 ppm, and the H_2/H_2O ratios will be in the range of 10 to 1000.

The general layout of the mechanical parts of the test apparatus has been completed. The detailing of the various parts is now in progress and fabrication will start soon. An alternative to direct dead-loading of the spacer normal to the rod axis is being examined. Sufficient space is available for a tungsten weight of 3 lb, which has been established as the maximum load; however, a lever-type system with a 10:1 ratio may be more conventient.

The gas-system layout has been reviewed and long-lead-time instrumentation has been ordered. The measurement of H_2O will be made with a Panametrics moisture monitor and the H_2:H_2O ratio will be measured with a Thermox meter. A check on the H_2:H_2O measurements will be made by reacting the H_2-H_2O mixture with hot CuO and measuring the amount of H_2O leaving the CuO and subtracting the amount of H_2O entering the CuO bed. The desired H_2O levels will be produced by reacting an He-H_2 mixture with CuO and mixing

with an He-H_2 mixture to produce the desired He-H_2-H_2O mixture. The He-H_2 gas mixtures will be passed through a molecular sieve and a charcoal trap chilled with liquid N_2 to remove any impurities. The holdup of H_2 in the charcoal trap is about one day and the gas will be passed through the trap in excess of one day to ensure equilibrium before starting the fretting tests.

During construction of the test apparatus and procurement of the instrumentation, a section of the gas system will be set up and used with existing instrumentation to determine the operating parameters to achieve the desired gas mixture.

3.2. FUEL-ROD ANALYSIS

During this reporting period, application of the LIFE-II code[3] to the analysis of the GCFR fuel rod has been focused on the phenomenon of fuel hot-pressing. To account for this phenomenon, a model is incorporated in the code that takes into account the densification of mixed-oxide fuel due to the application of an external pressure. In the LMFBR, this pressure is generated when the fuel comes into contact with the cladding and is forced against it by fission-product swelling in the burnup period before metal swelling causes the cladding to move away from the fuel. In the GCFR fuel rod with pressure equalization, the internal pressure is essentially the same as the external coolant pressure, or 85 atm. In the event that closed porosity would exist in the fuel, i.e., the external gas pressure could not be equalized within the pores of the fuel, this unbalance in gas pressure would generate a force that could cause hot-pressing of the fuel.

It was determined to look at this phenomenon from three aspects: (1) what the code predicts for the capsule GB-9 fuel rod irradiated in the ORR and how this prediction agrees with experimental evidence, (2) what the code will predict for the fuel behavior in the 300-MW(e) GCFR plant, and (3) the degree of closed porosity within the GCFR reference design fuel.

3.2.1. Effect of Initial Fuel Hot-pressing in the Capsule GB-9 Fuel Rod

Results from the thermal irradiation of the GB-9 fuel rod indicate negligible rod-diameter expansion at a burnup of about 5 at-%.

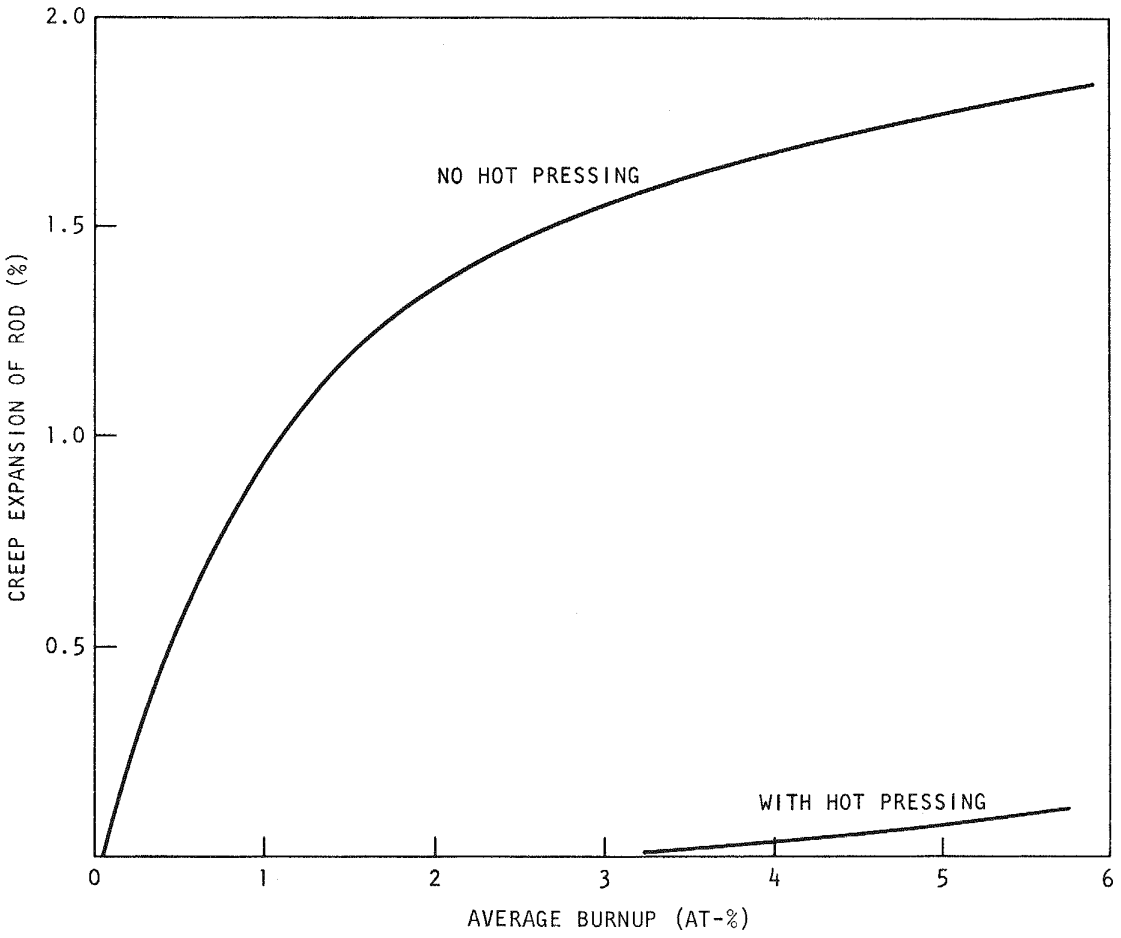

Fig. 3.14 Predicted expansion of GB-9 fuel rod

The predicted rod-diameter expansion versus burnup for the GB-9 fuel-rod conditions using the LIFE-II code is plotted in Fig. 3.14. Assumptions for the calculation are listed in Table 3.3. With hot-pressing, the predicted expansion is negligible, whereas without hot-pressing the predicted expansion at 5 at-% burnup is 1.8% of the diameter.

Since the experimental results show negligible diameter increase up to 5 at-% burnup, it appears that early hot-pressing of the fuel may be important in delaying fuel-cladding contact. Unfortunately, it is not possible to visually assess the degree of hot-pressing from metallographic

Table 3.3

CAPSULE GB-9 IRRADIATION CONDITIONS

Pellet inside radius, in.	0.300
Pellet outside radius, in.	0.1505
Cladding inside radius, in.	0.1522
Cladding outside radius, in.	0.1765
Pressure, psi	
Inside	1000
Outside	1000
Fuel fabricated density, % theoretical	92.4
Rod rating, kW/ft	15.5
Cladding inside temperature, °F (°C)	1356 (735)
Heat flux in rod, maximum to minimum	2.4

sections of the GB-9 fuel rod since, as shown in Fig. 3.14, at 5 at-% burnup even with hot-pressing, the fuel has expanded out to the cladding. Observations at very low burnups are required.

3.2.2. Effect of Initial Hot-pressing on Fuel Temperatures in the GCFR

The GCFR reference design has a conservatively low maximum fuel-rod rating of 12.5 kW/ft in order to avoid centerline melting, even with 10% overpower. However, the low centerline temperature depends on a reasonable value for the fuel-to-cladding thermal conductance, which is typically assumed as 2000 Btu/(ft^2)(hr)(°F). This value is observed in fuel rods in

which there is contact of the fuel and cladding. However, there may be a considerable period of operation before fuel-cladding contact is established by swelling of the fuel. During this period, centerline melting is possible. This initial operational period of the fuel rod as it is affected by the fabricated fuel-cladding gap and the operating cycle was studied with the LIFE-II code. For an open gap, the thermal conductance in the LIFE-II program is given as

$$H_G = 317 + \frac{0.312}{G + 0.000226} \text{ Btu/(ft}^2\text{)(hr)(°F)},$$

where G is the radial gap between the fuel and cladding in inches. For a zero gap,

$$H_G = 1700 \text{ Btu/(ft}^2\text{)(hr)(°F)}.$$

Conditions for the calculation are given in Table 3.4. Cladding swelling was set equal to zero in order to give the fuel the best chance to reach the cladding and thus increase the contact conductance.

Table 3.4

REFERENCE-DESIGN FUEL ROD FOR LIFE-II STUDY

Pellet inside radius, in.	0.0244
Pellet outside radius, in.	0.1218
Cladding inside radius, in.	0.1238
Cladding outside radius, in.	0.1423
Outside pressure, psia	1250
Inside pressure, psia	1250
Fuel density, % theoretical	0.86
Cladding surface temperature, °F (°C)	1124 (611)
Rod heat rating, kW/ft	12.55

The results of two calculations of the fuel-cladding gap as a function of fuel burnup are shown in Fig. 3.15. The smooth curve represents a steady-state run at 12.55 kW/ft. The circled points represent a cyclic run with six drops in power to 3 kW/ft followed by immediate increase to 12.55 kW/ft. The purpose of the cyclic run was to explore the possibility of a fuel ratchetting mechanism,[3] involving cracking and healing, which might increase the rate of fuel expansion. The cycling obviously had a negligible effect

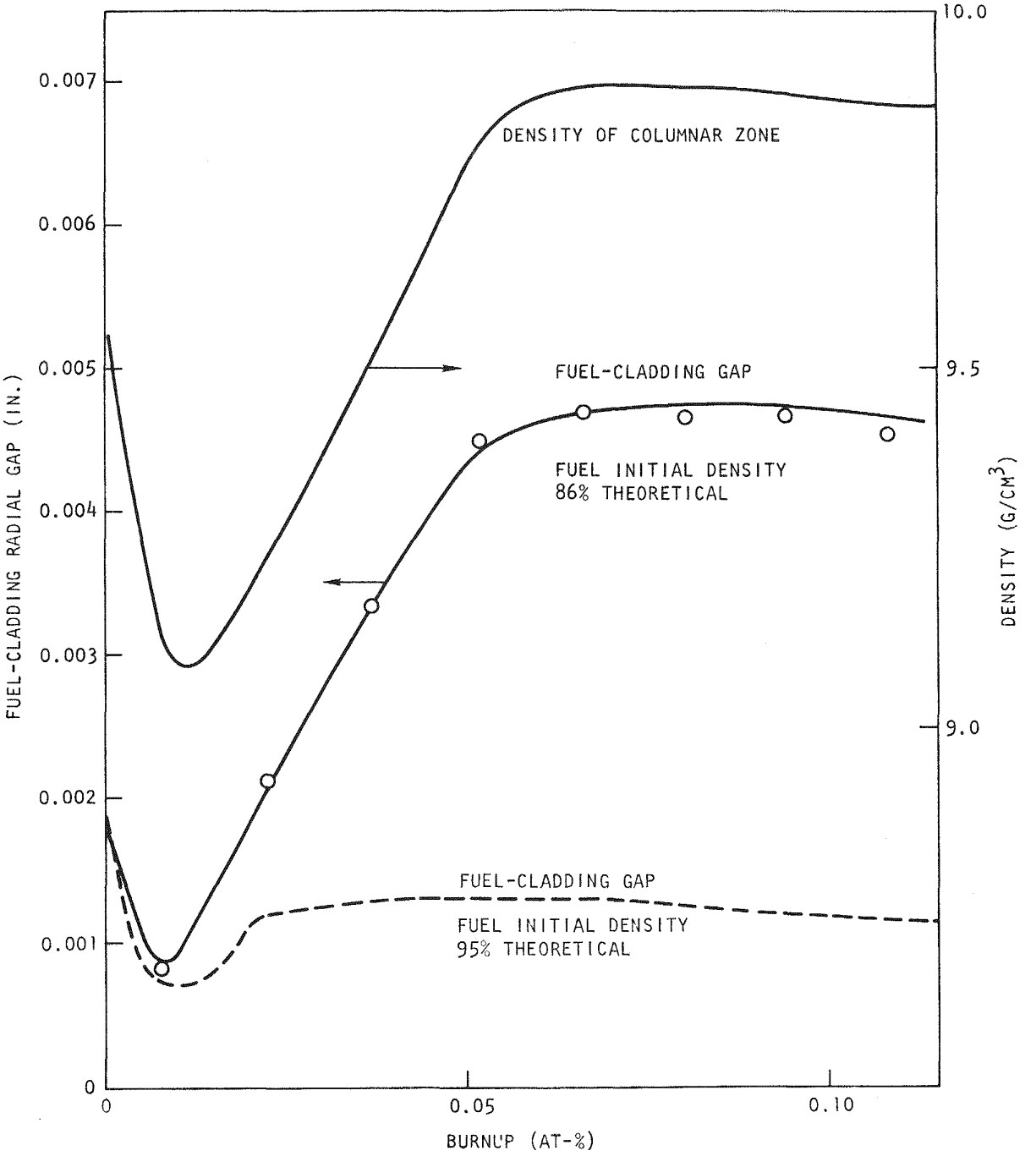

Fig. 3.15 Fuel-cladding gap and fuel density at low burnup

on the rate of gap closure. On the same plot the fuel density is also shown, illustrating the initial hot-pressing that delays the fuel-cladding gap closure.

During this initial period, the central temperature increases rapidly from 4600°F to 5100°F (see Fig. 3.16) as a result of the low thermal conductance of the open fuel-cladding gap. Later, the temperature gradually falls as the fuel-cladding gap diminishes, but it remains above the melting point to 1 at-% burnup. The calculation was repeated for a fuel fabricated density of about 95% of theoretical; these results are shown as dotted curves on Figs. 3.15 and 3.16. The high initial density practically eliminates the hot-pressing effect and the resulting initial increase in central fuel temperatures.

It would appear from these results that a low initial fuel density, which permits hot-pressing and delays the expansion of the fuel to the cladding, may be a drawback. Another possibility, however, is that hot-pressing may not occur in the manner that this code predicts and that this initial increase in the fuel-cladding gap is not real. In any case, it seems that the early stages in fuel irradiation may be critical in determining fuel lifetime.

3.2.3. Study of Method of Calculating Hot-pressing in LIFE-II Code

The calculations of fuel hot-pressing in LIFE-II assume that mechanical confinement and hydrostatic gas pressure produce the same hot-pressing effects. This would be strictly true only if porosity is in the form of unconnected bubbles so that gas pressure cannot equalize through the solid by capillary flow.

Measurements of open porosity in uranium oxide pellets of 91% theoretical density (TD) were performed by mercury porosimetry and BET surface-area measurement techniques. The results are as follows:

1. Mercury porosimetry on a UO_2 pellet of 90.9% TD showed open porosity volume of 0.004 cm^3 in a total pellet volume of 2.947 cm^3.
2. The BET surface area based on krypton adsorption on a UO_2 pellet of 91.2% TD was measured to be 260 cm^2 compared to a geometric surface area of 2.583 cm^2.

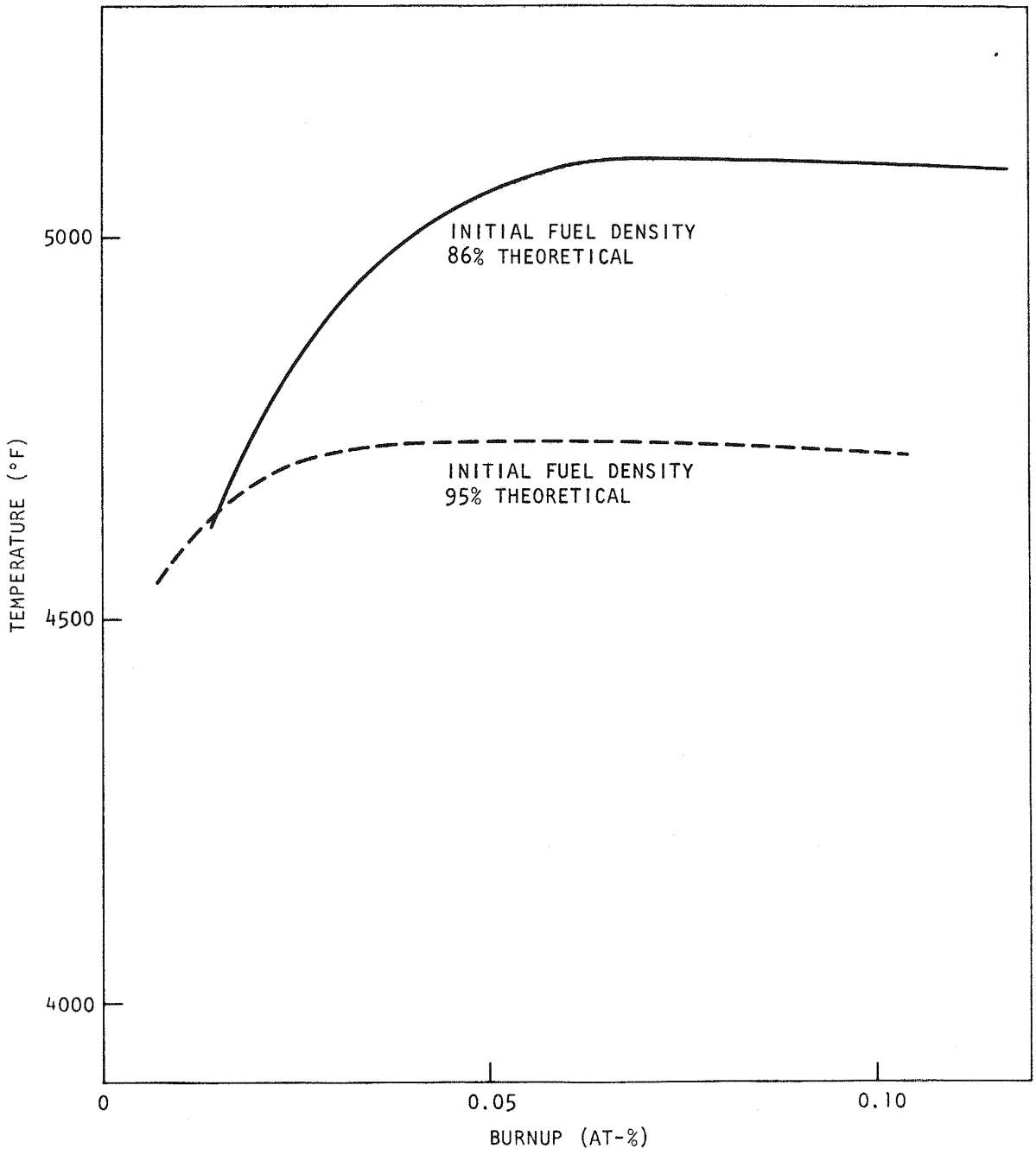

Fig. 3.16 Maximum fuel temperature at low burnup

Even though these low values for open porosity are probably representative of both uranium oxide and mixed-oxide fuels, which are pressed and sintered without binders, it should be kept in mind that oxide fuel made by employing binders or preslugging may yield quite different results.

The low proportion of connected porosity tends to confirm the LIFE-II assumption that gas hydrostatic pressure will not come to equilibrium by penetration of the solid pores.

3.2.4. Conclusions

Measurements on UO_2 of about 91% TD have shown that most of the fuel porosity is closed. These measurements are considered representative of mixed oxides, and this closed porosity will lead to a pressure inbalance between the exterior and interior of the fuel under the high pressure to which GCFR fuel is subjected. A hot-pressing model in the LIFE-II code predicts that this pressure inbalance would lead to fuel densification with a resulting increase in the fuel-to-cladding gap and in the fuel centerline temperature.

Comparison of predictions from application of the LIFE-II code to the measured diametral growth of the GB-9 fuel rod suggests that fuel hot-pressing may have occurred. Visual observations at higher burnups are not useful, since even with hot-pressing, the gaps are closed. However, observations at low burnups would be useful to further characterize fuel behavior.

In Section 5.1.2, measurements of the time dependence of pressure drops in the vented-fuel-rod irradiation test of the GB-10 fuel rod are described. A transient increase in the pressure drop during initial startup and approach to the 12 kW/ft power level is suggestive of the fuel-to-cladding gap closing. Other recent results[9] indicate that gap closure should have occurred during startup with the small initial diametral gap (0.003 in.) in the GB-10 fuel rod. However, the subsequent decrease in pressure drop in GB-10 can be explained by several models, not necessarily including the phenomenon of hot-pressing. Fuel behavior during the early stages of irradiation still seems quite ill-defined, and the model being used in LIFE-II should be refined based on actual experimental evidence.

The importance of this potential phenomenon is illustrated by its calculated effect on fuel rods for the GCFR reference design, in which centerline melting would be predicted if low density (86% TD) fuel were used at the reference linear heat-generation rating of 12.5 kW/ft. However, the use of higher-density (95% TD) fuel practically eliminates hot-pressing and the resultant increase in central fuel temperature.

These results indicate the importance of

1. Improving the LIFE-II hot-pressing model, which is now based on simple tests with Al_2O_3.
2. Obtaining results from short-time irradiation tests in which the effect of hot-pressing would be most easily observed.
3. Investigating the irradiation behavior of higher-density (~95% TD) fuels.

3.3. MONITOR STATION INSTRUMENTATION

Development of the monitor station instrumentation is required at an early date in order to verify the analytical model being developed. The most direct means of testing the instrumentation is by coupling it to vented-fuel-rod irradiation experiments. The capsule GB-10 fuel rod (a vented rod) is already being tested (see Section 4.1.2) and tests of a 12-rod vented bundle in the BR-2 reactor at Mol, Belgium, are scheduled to begin in early 1974. Therefore, the preliminary work should be initiated immediately in order to complete the development of the instrumentation in time to take advantage of these experiments, which are the only vented irradiation experiments currently scheduled.

During this reporting period, work was initiated on the modification and further development of the computer program for the monitor station instrumentation. The computer program COUNT that is being modified for this purpose was initially developed with private funding to make a preliminary assessment of the possibilities of detecting leaking fuel elements and monitoring the leak progression. A brief description of this program is given below.

The basic purpose of COUNT, which is written in FORTRAN V language, is to calculate the count rate and energy spectrum to be observed in a monitor

station resulting from activity in the sweep gas flowing through the pressure equalization system lines from the core of the GCFR to the helium purification system. The steady-state condition count rates before and after the onset of one or more leaks in the fuel elements of the core are computed. Prior to the advent of a leak in the cladding of the fuel rods, the transport time is dominated by gaseous diffusion of fission products from the fuel to the top of the elements where the fission products are picked up by the sweep gas and carried through the lines. When a leak occurs, transport in the leaking rod is by inleakage of gas into the fuel region to the sweep-gas entry point and then through the pressure equalization system. The change in the decay time (transport time) between the fuel and the counting station determines the activity level in the line. It is assumed in the calculations that equilibria conditions exist with respect to solid-state diffusion or migration of fission products in the oxide fuel matrix, radioactive buildup and decay, sweep- and leak-gas flow conditions, and gaseous diffusion conditions. Activity of each fission product of interest is computed separately and then summed to arrive at a total count rate. Conversion of beta particles to bremsstrahlung in the wall of the piping is accounted for. Attenuation by shielding is included. The energy dependence of the attenuation is handled with a subroutine in which interpolation between data points in a table is provided. The effects of size and location of the sodium iodide detector as well as sensitivity effects are also included. Input activities are provided by previous RAD2[10] calculations and gaseous diffusion delay times are estimated using the SLIDER[11] program or are assumed on the parametric basis. Transport times during convection flow are based on system volumes and the assumption of slug flow through them. Alternatively, experimental values of convection transport time may be used where available (e.g., from the GB-10 fuel rod irradiation experiment). The output consists of the identification of each isotope, its count rate from a leaking rod, from a nonleaking element, and from a leaking element, and the summed totals of the activities of all of the isotopes from each of these sources. Finally, the ratio of total activity from the leaking conditions to nonleaking conditions is printed.

Initial modification of COUNT will include an option to use the model of the ionization chamber instrumentation currently installed in the GB-10 capsule sample line. Additional modifications to be made will include the necessary geometric factors to design a collimator that can be used with the sodium iodide detector and the introduction of a library of oxide-fuel-matrix release fractions for the GB-9, GB-10, and 300-MW(e) GCFR plant fuel rods. Spectral output and monitor-line connection information will be added at a later time.

3.4. LOWER SHIELD ASSEMBLY

A draft of the topical report summarizing the conceptual design analysis for the GCFR lower shield assembly was completed and the report is being prepared for publication.

A layout of the concept of multiple layers of trays for containment and cooling of gross core melting was initiated for the purpose of evaluating its feasibility for the GCFR reactor system.

Additional criticality investigations were carried out using a one-dimensional spherical model for the design basis of one or several elements melting. This investigation included the following conservative assumptions: (1) the elements form a porous sphere of UO_2-PuO_2 with a uniformly distributed void of 50%, which is the helium coolant volume fraction of a GCFR fuel element, (2) the additional stainless steel volume fraction (~16%) was neglected, and (3) the enrichment used was Zone 4 of the GCFR reference design, which is 22.1%. The variables used were (1) the number of elements melted and (2) a bare sphere versus a fully reflected sphere. These results were compared to previous calculations reported for fully compacted spheres of condensed UO_2-PuO_2 fuel. For the fully reflected case, three elements condensed into a 50% porous sphere are required to achieve criticality, whereas only one element was required for a fully compacted sphere. For the case of an unreflected porous (50% void) sphere, it takes over ten elements to achieve criticality compared to about two elements for a sphere of fully compacted UO_2-PuO_2 fuel. It is concluded from this study that secondary criticality from melting of a few elements is not expected.

REFERENCES

1. Sutherland, W. H., and V. B. Watwood, Jr., "Creep Analysis of Statically Indeterminate Beams - CRASIB, Users Guide and Program Manual," USAEC, Report BNWL-1362, Battelle Northwest Laboratories, June 1970.

2. Brown, C. A., R. K. Dawless, and P. J. Levine, "Data Package for Unencapsulated Fuel Pin Irradiation Tests in EBR-II Grid Type Subassembly WSA-4," USAEC, Report WARD-242, Westinghouse Advanced Reactor Division, February 1972, pp. A-9 and A-10.

3. Jankus, V. Z., and R. W. Weeks, "LIFE-II—A Computer Analysis of Fast-reactor Fuel-element Behavior as a Function of Reactor Operating History," Nucl. Eng. Design, Vol. 18, No. 1, 1972, pp. 83-96.

4. "GCFR Quarterly Progress Report for the Period February 1, 1972 through April 30, 1972," USAEC, GA-A12165, Gulf General Atomic, July 20, 1972, p. 21.

5. Horvay, G., "The Plane-Stress Problem of Perforated Plates," ASME J. Appl. Mech., Vol. 19, September 1952, pp. 355-360.

6. Roark, R. J., Formulas for Stress and Strain, McGraw-Hill Book Company, 1955.

7. Rowe, D. S., "COBRA-II: A Digital Computer Program for Thermal-Hydraulic Subchannel Analysis for Rod Bundle Nuclear Fuel Elements," USAEC, Report BNWL-1229, Battelle Northwest Laboratories, February 1970.

8. Ingesson, L., and S. Hedberg, "Heat Transfer Between Subchannels in a Rod Bundle," Fourth International Heat Transfer Conference, Paris, Vol. III, 1970, Paper FC 7.11.

9. Ballard, E. O., et al., "Linear Heat Rating for Incipient Fuel Melting," Transactions, American Nuclear Society, Vol. 15, 1972, pp. 752-54.

10. Vanslager, F. E., "RAD2, A Computer Program for Calculating Fission-product Radioactivities," USAEC, Report GAMD-6908, General Dynamics Corporation, General Atomic Division, July 23, 1965.

11. Jadhov, K. B., and B. W. Ross, "SLIDER, A FORTRAN V Program for the Computation of the Release of Fission Products from One-dimensional Multilayered Fuel Configurations," USAEC, Report GA-8566, Gulf General Atomic, August 1, 1969.

4. TASK 4160—PRESSURE EQUALIZATION SYSTEM FOR FUEL

Work on the development planning document for the pressure equalization system has been initiated, an outline has been prepared, and a format is being established that will comply with applicable RDT standards.

5. TASK 4200/4400—FUELS AND MATERIALS DEVELOPMENT

5.1. THERMAL-FLUX IRRADIATION EXPERIMENTS

5.1.1. Postirradiation Examination of Irradiation Capsule GB-9

Postirradiation examination (PIE) of the vented fuel rod (see Fig. 5.1) irradiated in ORR capsule GB-9 to ~54,000 MWd/Te is continuing at Argonne National Laboratory (ANL).

Electron microprobe analysis of the transverse metallographic sample taken 4-3/16 in. above the bottom of the fuel column has been completed. The results of the microprobe analysis of selected areas of cladding attack was summarized in the previous progress report.[1] Radial point-counting traverses across the fuel for zirconium, cesium, uranium, and plutonium have resulted in distributions of these elements that substantiate the calculated radial power production.[2] It was found that there was approximately 2-1/2 times more zirconium near the outer surface of the rod than there was near the central void, which indicated that the reduction in burnup near the central void resulted from self-shielding in this rod irradiated in a thermal flux. The radial burnup profile from the hot side (the side nearest the reactor core) to the cold side was also shown by the radial distribution of zirconium. The zirconium content on the hot side of the element was approximately 1-1/2 times higher than that on the cold side. The plutonium distribution also indicated a burnup gradient across the rod, in that less plutonium remained on the high-burnup (hot) side than on the low-burnup (cold) side. The cesium distribution was the reverse of the zirconium distribution; slightly more cesium was found on the cold side than on the hot side, indicating that cesium migrated to the cooler side of the rod. The most severe cladding attack also occurred on the cold side of the rod at this axial position.

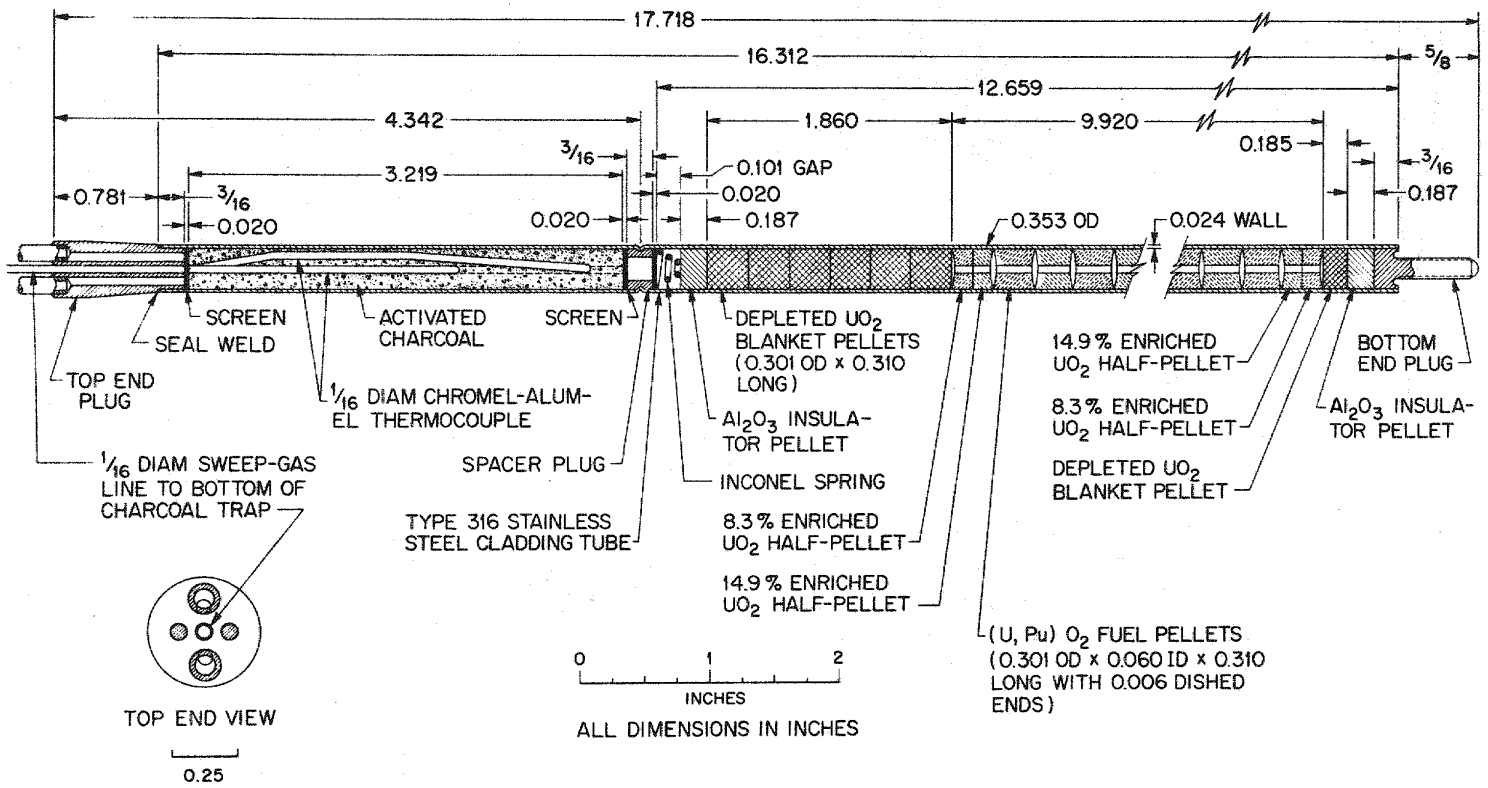

Fig. 5.1 GCFR fuel rod in capsule GB-9

Optical metallography was performed on five axial positions along the fuel region of the GB-9 fuel rod. Attack of the cladding adjacent to the fuel was observed in each section except that taken at the bottom of the rod. The maximum attack penetrated approximately 0.006 in. into the cladding. The attack was intergranular at its leading edge, but all of the grains were consumed by the reaction nearer the fuel-cladding interface, as shown in Fig. 5.2. Examination of the longitudinal sections at the ends of the fuel column indicated that relatively large amounts of fission-product cesium were present adjacent to the cladding. The relatively low cladding temperatures, less than 500°C, at the bottom of the fuel column prevented attack from occurring in that region of the rod. The maximum attack occurred in the region of the 14.9% enriched UO_2 half-pellet at the top of the mixed-oxide fuel column, as shown in Fig. 5.3. This figure is a composite of photomicrographs of the top longitudinal section of GB-9 and shows that the central hole has closed at the top of the 14.9% enriched UO_2 half-pellet. The fuel pellets (both 14.9% and 8.3% enriched UO_2 pellets and the mixed-oxide pellets) were fabricated with a 0.060-in.-diam central hole. At the bottom of the fuel column, the central hole has narrowed, but it has not been completely closed off by fuel, as shown in Fig. 5.4. Based on the microprobe analysis results, the closing of the central hole appears to have resulted from fuel being vaporized in the hotter regions of the rod and being condensed in the cooler regions at the ends of the fuel column. The central hole was enlarged and displaced toward the hot side of the fuel rod except at the bottom of the column of mixed-oxide fuel pellets. No cesium was found in the constricting deposit; cesium was found only in the outer (~1/3) of the fuel and in axial locations beyond the constrictions where temperatures during irradiation were lower than in the fueled region. Continuous gamma scans for cesium in the fuel-blanket interface region have been obtained by ANL, but the scan results have not yet been received at GGA.

Since the sectioning of the GB-9 fuel rod in the upper and lower blanket interface regions has revealed constrictions of the central hole in the fuel column, it was necessary to review the flow testing done on the GB-9 fuel rod. Because of difficulty in drilling tap holes into the central hole at

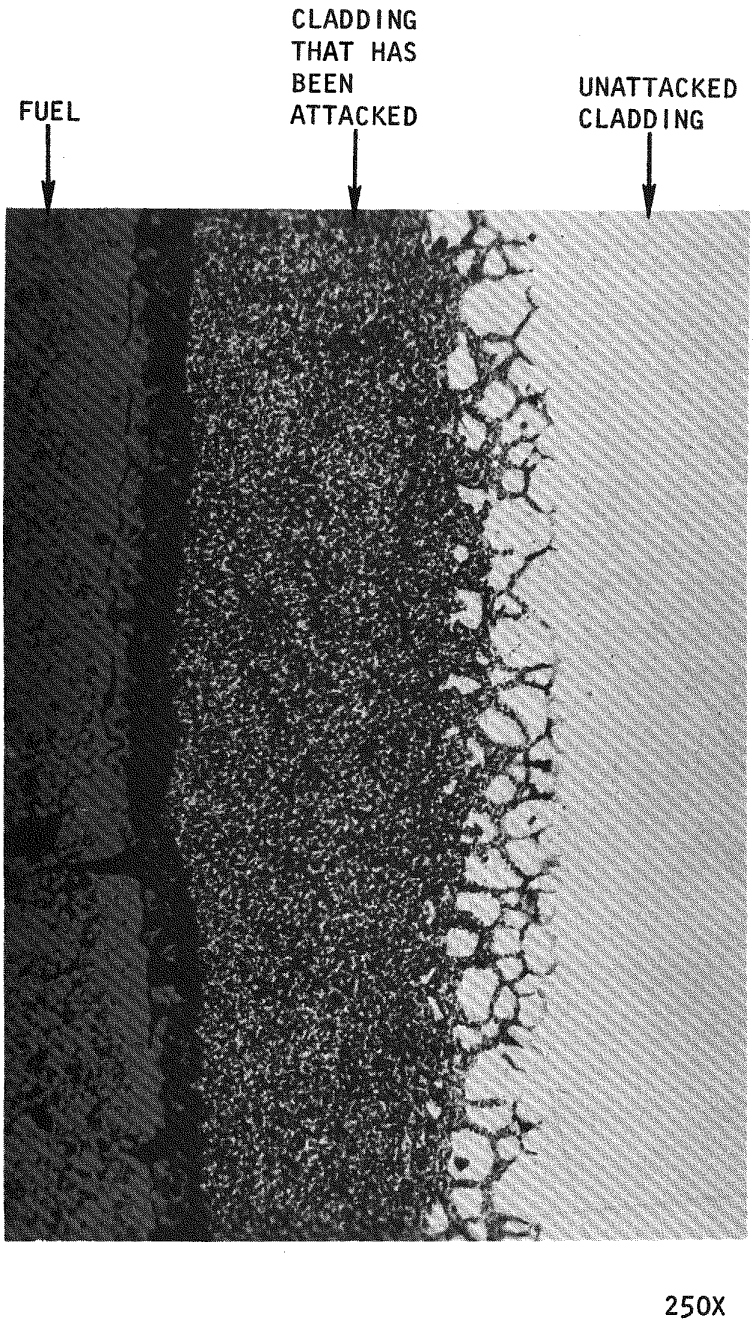

Fig. 5.2 Area of the most severe cladding attack near the top of the fuel column of GB-9 fuel rod

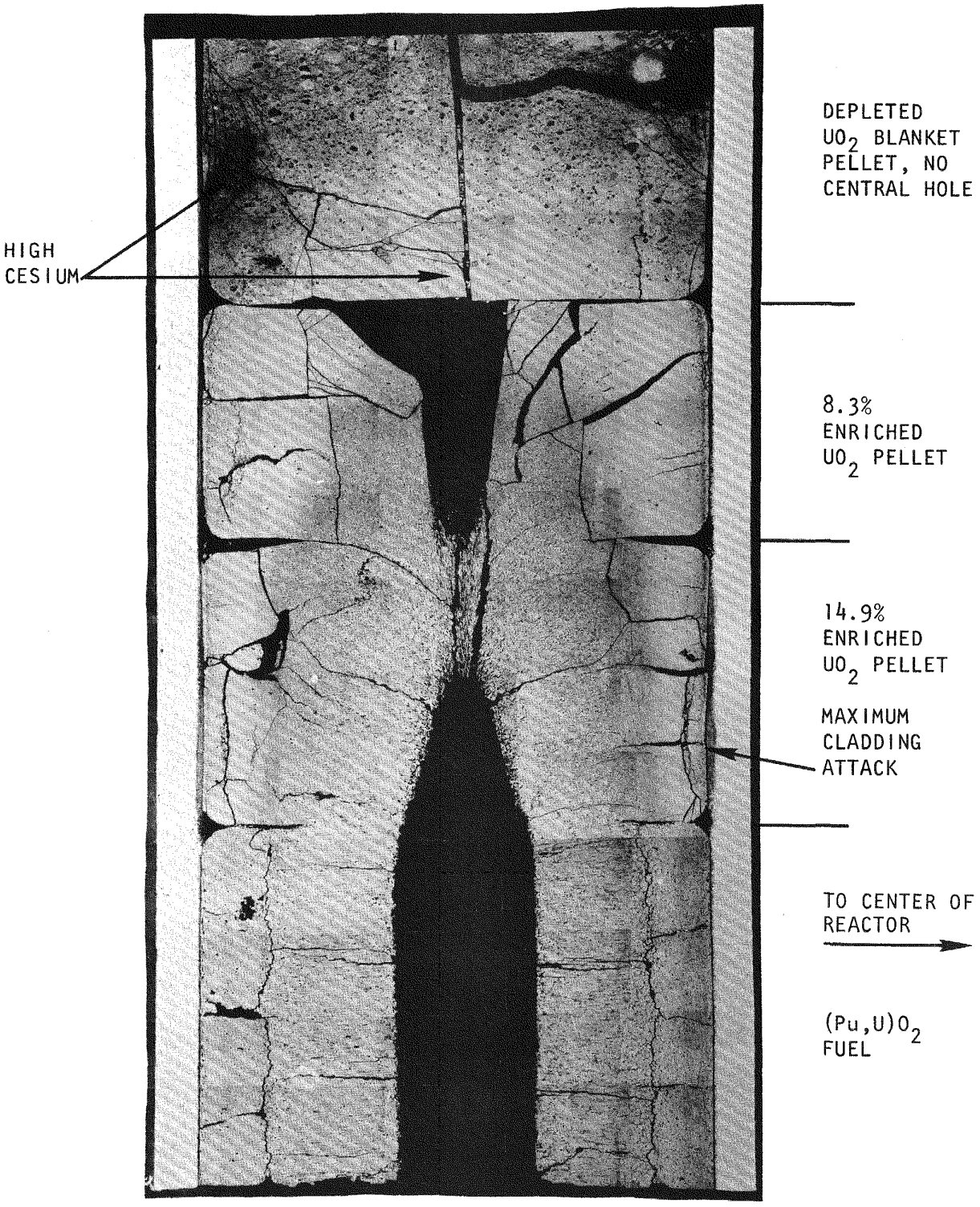

Fig. 5.3 Longitudinal section of the GB-9 fuel rod at the top of the fuel column

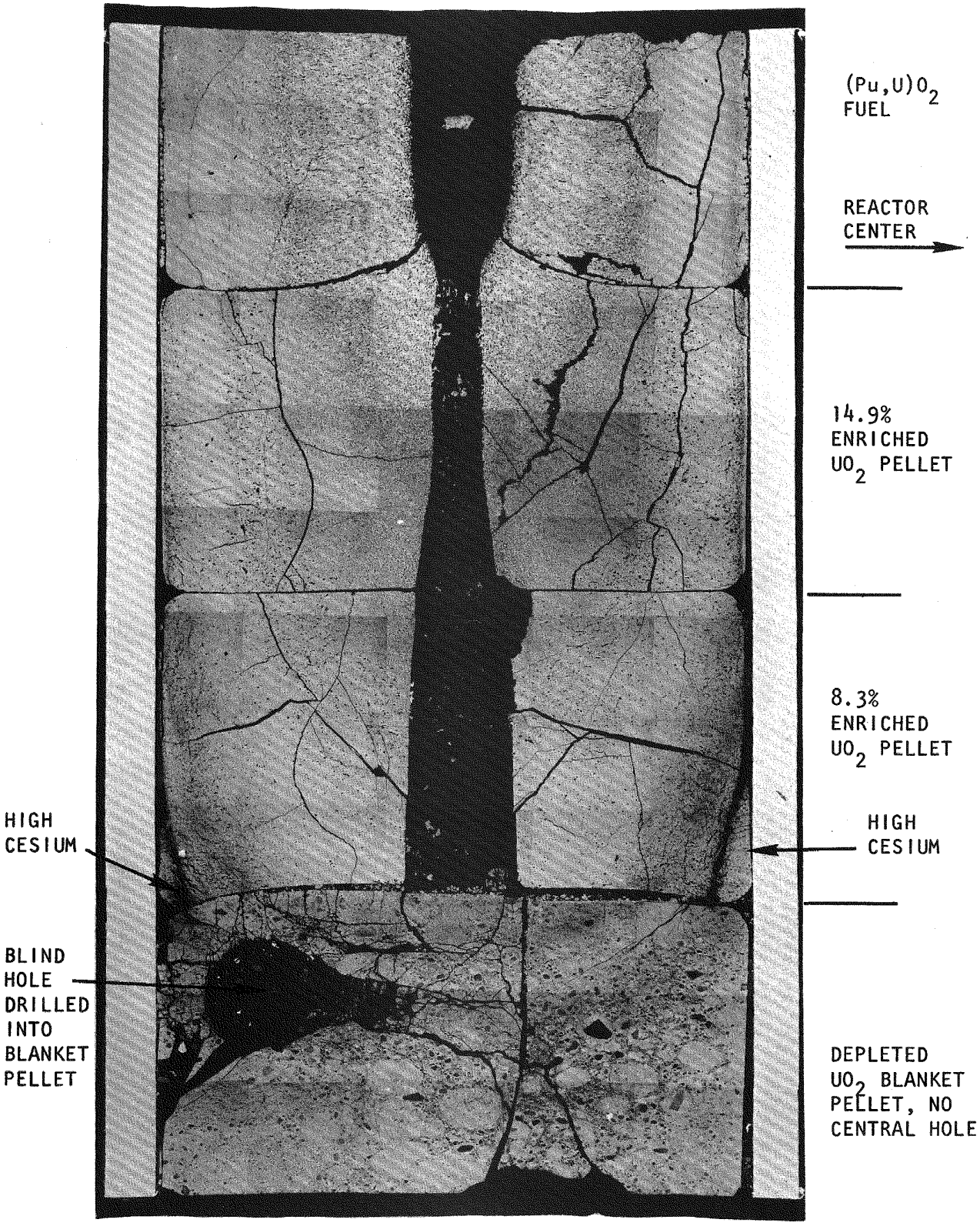

Fig. 5.4 Longitudinal section of the GB-9 fuel rod at the bottom of the fuel column

the ends of the fuel column, additional holes were drilled farther along the fuel column and these bypassed the constricted areas shown in Figs. 5.3 and 5.4 Thus, the data previously reported (Fig. 4.1 of Ref. 1) should not have been corrected to the total fuel length. There were no measurements made on the resistances to gas flow through the constricted areas by themselves. However, data are available that provide information on minimum flow through these regions. The applicable data are listed in Table 5.1.

With respect to the first entry, the test-flow gas entered a blind hole in the blanket pellet of the rod just below the fuel (see Fig. 5.4) and passed through the lower constricted region and the upper constricted region to the top interface between the fuel column and the upper blanket. With a pressure differential of 50 in. of water, or approximately 2 psi, a flow of 0.1 cm^3/sec was observed. A separate measurement over this flow path was made by taking the pressure decay of the known gas volume, which confirmed the magnitude of the flow observed. When these observations are considered with those for the fourth entry, the resistance appears to be mostly that of the blind hole to entry of the test gas.

A third measurement in which gas passed through or around the constricted regions is shown by the data in the last entry in Table 5.1. In this case, the test gas entered the central hole of the fuel column above the lower constriction and passed through the lower constriction and out a hole at the lower fuel-blanket interface and also passed upward through the upper constriction to the upper fuel-blanket interface. With a pressure differential of 40 in. of water, or approximately 1-1/2 psi, a flow rate of 0.9 cm^3/sec was measured. In view of the results of measurements in these two flow modes, which indicated that the gas passed through the constricted regions, it is apparent there was sufficient flow to permit pressure equalization of the fuel rod, even in the central hole of the fuel region, in less than 1 min with approximately 2 psi pressure differential being applied. Since the purpose of pressure equalization is to avoid creep strain of the cladding, the measured flow rate is satisfactory and provides a large safety margin for this application.

Table 5.1

HELIUM FLOW TESTS THROUGH THE FUEL REGION OF GB-9 FUEL ROD

Location of Entrance Hole(s)[a] (in.)	Location of Exit Hole(s)[a] (in.)	Pressure Loss[b] (in. of H_2O)	Flow Rate (cm^3/sec)
1/2 (lower blanket)	10-7/16 (bottom of upper blanket); 12-5/8 (bottom of trap)	50	~0.1[c]
2-1/2 (fuel)	1/2 (lower blanket); 10-7/16 (bottom of upper blanket); 12-5/8 (bottom of trap)	50	1.2
2-1/2 (fuel)	10-7/16 (bottom of upper blanket); 12-5/8 (bottom of trap)	50	1.2
2-1/2 (fuel)	1/2 (lower blanket)	50	~0.1
1-1/4 (fuel)	1/2 (lower blanket); 10-7/16 (bottom of upper blanket)	40	0.9

[a]The locations of the holes were measured with respect to distance above the weld closure of the bottom end cap. All holes were 0.085 in. in diameter and were drilled to the pellet centerline.

[b]Pressure loss was measured by the pressure difference between a point at the entrance hole pressure and ambient pressure. In several cases, more than one exit and thus more than one flow path is involved.

[c]This flow was also confirmed by pressure decay test.

To determine the effect of the irradiation on the properties of the cladding, biaxial stress-rupture tests at 700°C were performed on a section of the Type 316 stainless steel cladding of the GB-9 fuel rod (taken from the fueled region) and on two tube samples of the same material in the unirradiated condition. The results are summarized below. The amount of loss in rupture life and ductility agrees with values reported in the literature for SA 316 stainless steel.

Sample No.	Test Condition		Rupture Life (hr)	Average Rupture Strain (% ΔD/D)
	Pressure (psig)	Stress (psi)		
Unirradiated No. 1	3,600	22,900	46-1/4	16.4
Unirradiated No. 2	3,450	22,000	57	16.8
GB-9 cladding	3,450	22,000	1/2	3.3 (preliminary estimate)

The metallography of samples located near the GB-9 stress-rupture specimen exhibited fission-product attack up to a depth of 4.4 mils into the cladding, and it was suspected that the attack may have contributed to embrittlement and the short GB-9 rupture life, but since other workers have shown similar results in the absence of attack, it appears that the attack did not have a major effect on the rupture life of the GB-9 stainless-steel cladding.

5.1.2. Irradiation Capsule GB-10

Irradiation of the vented-fuel-rod, sweep-gas capsule experiment GB-10, which started on August 29, 1972, has reached a burnup of more than 4,200 MWd/Te. The rod is being operated initially at a linear heat rate of 12 kW/ft until steady fission-gas release conditions are attained (at approximately 10,000 to 15,000 MWd/Te). After this initial period, the heat generation rate will be increased to 15 kW/ft for the remainder of the exposure to a burnup goal of 75,000 MWd/Te.

Startup of GB-10 was delayed for approximately three weeks because significant amounts of moisture were detected in the sweep-gas system. A valve was installed to permit evacuation of the system and after several pressurization and evacuation cycles, the moisture level was reduced to satisfactory values. Upon startup of the capsule irradiation, the sweep-gas inlet monitor indicated 0.04 ppm moisture and the monitor downstream of the fuel indicated 1 ppm moisture. No change in moisture monitor ratings was indicated during the capsule rise to power to 12 kW/ft. It is not known whether the two moisture levels indicated by the instruments are real differences since they were measured at the lower limit of the instrument range. Further work will be required to elucidate this point. On the second day after startup, fission-product activity was monitored during several sweep gas flow modes; the results are tabulated below. In addition, fission-gas samples were taken during the various flow modes.

Sweep-gas Flow Modes at 1000 cm^3/min	Steady-state Activity (mr/hr)
In and out through top of fuel rod trap	5.5
In through top of trap, out through bottom of trap	14.8
In through top of trap, out through bottom of blanket	72
In through bottom of fuel, out through top of trap	456
In through bottom of fuel, out through bottom of blanket	558

The results for the sweep-gas flow were analyzed with the COUNT code (described in Section 3.4) by calculating the ratio of activity in the sample line in the swept fuel mode to the activity occurring during sweeping gas in and out of the top of the trap. Calculated and measured ratios for these two sweep modes are 71.5 and 82.9, respectively. In program COUNT, it is assumed that solid-state diffusion, gaseous diffusion, and radioactive and flow equilibria conditions prevail. It should be noted that solid-state diffusion and radioactive equilibrium have not yet been obtained in capsule GB-10, and thus the analysis is only preliminary.

Convective flow transport times were measured in capsule GB-10 to be ~50 sec from the capsule to the sample-line monitors, and this value was used as COUNT input. An irradiation time of 1 yr was also assumed in the

COUNT input. The procedure followed was to adjust the gaseous diffusion transport time input to COUNT so that the computed ratio of the activity detected by the sample-line monitor would approximate that measured in GB-10. A value of 12 hr was found to be fairly close and was selected because that time had been indicated as the most likely gaseous diffusion transport time in capsule GB-9.

During initial startup and approach to the 12 kW/ft power level, some unexpected deviations were observed in (1) the pressure differential across the fuel rod and the 80-ft lead lines while sweeping helium gas through the fuel rod and (2) the readings of the thermocouples monitoring the cladding temperature. During this period with a BF-TT flow mode and the gas flowing approximately 1000 std cm^3/min through the fuel rod and lead lines, the pressure differential across the lead lines, measured at the valve box, rose from a preirradiation value of approximately 8 psi to 65 psi, oscillated to 19 psi and to 34 psi, and then gradually stabilized at a value of 8 to 10 psi. At the same time, two thermocouples monitoring the cladding temperature became unsteady, with oscillations as much as 20°C and with the maximum temperature reading shifting from one to the other thermocouple and back again. As the irradiation has proceeded since that time, both the pressure differentials and the temperatures have been steady but the activity level measured by the sample-line monitor has fallen by more than a factor of 10. A review of the very early GB-9 sample-line-monitor data also indicated an initial rise in activity, followed by reduction by a factor of 2, and then the long-term rise usually shown. At the lower heating rating (12 kW/ft versus 16 kW/ft), the transient period may be longer and the steady activity level somewhat lower. The activity level at the sample-line monitor in GB-10 has not yet started to rise again. The reasons for the above observed phenomena are not known, but it is speculated that they are associated with thermal-mechanical changes in the fuel, including closing of the fuel pellet-to-cladding gap, restructuring of the fuel to form a central hole, and changes in the temperature distribution and affected volumes of the rod.

5.2. FAST-FLUX IRRADIATION EXPERIMENTS

5.2.1. F-1 (X094A) Fast-flux Irradiation Experiment

Irradiation of the F-1 subassembly of seven encapsulated fuel rods in EBR-II has reached exposures up to ~44,000 MWd/Te toward the goal of 100,000 MWd/Te.

The postirradiation examination of capsule G-3, which was removed from subassembly X094 during the interim examination at 27,000 MWd/Te, is continuing. Disassembly was performed and the fuel rod has been removed from the capsule tube and thermal barrier. Visual examination of the fuel rod did not reveal any significant unusual features. An attempt was made to detect cladding-fission product attack by an eddy current test; however, the results are inconclusive, although there was some indication of attack on the inside of the cladding. The cladding used for the G-3 fuel rod is thicker than that which has previously been measured by eddy-current testing at ANL, so the equipment calibrations were for thinner tubes. As a consequence, two samples of cladding used for the F-1 experiment have been sent to ANL for making calibration samples for the eddy current testing on cladding of the proper thickness. Profilometry of the fuel-blanket section of the G-3 fuel rod has been completed and it shows that only a maximum increase of 0.0004 in. (0.13%) over the original nominal dimensions occurred. The cutting diagram and flow-testing procedures for the G-3 rod were agreed on between GGA and ANL and the work will commence in November 1972.

Analysis of gamma spectrometry data from the interim analysis of two rods of the F-1 (X094A) experiment continued. Some results were reported in the previous quarterly report.

The expected diametral profile for a nonvolatile species as a function of the diametral distance across a fuel rod was recalculated and an error was found in the data previously reported.[1] Although the general shape of the profile remains the same, there are quantitative differences. The recalculated profile, assuming uniform fission-product distribution and a 0.60-in.-diam central hole, is shown in Fig. 5.5.

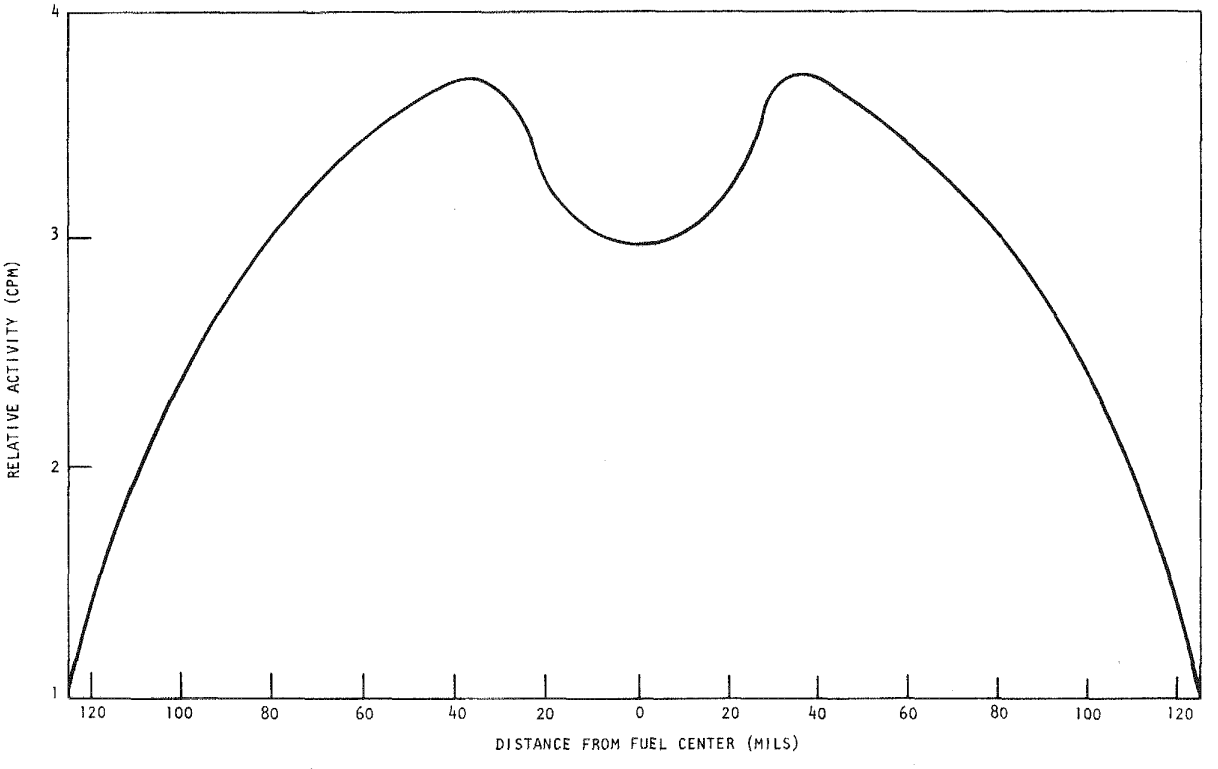

Fig. 5.5 Diametral gamma activity profile of an F-1 fuel pellet

The five replacement fuel-rod capsules for the F-1 (X094A) experiment have been shipped from ORNL to EBR-II and the data package containing the "as-fabricated" details of the capsules is being prepared.

5.2.2. F-3 Fast-Flux Irradiation Experiment

The design and operating conditions of the GGA fuel rod capsules to be irradiated in the F-3 EBR-II experiment, which is to be shared with the ANL Group 08 experiment, was reviewed by members of the Fuel Performance Section and of the Fuel Element Fabrication Section of the Materials Science Department of ANL and by personnel of the GCFR Project on September 28, 1972.

Some proposed design changes in the F-3 fuel-rod capsule were made by ANL to make it more like the Group 08 fuel-rod capsule design for the purpose of allowing similar means for fabrication and handling of the fuel-rod capsules for both experiments. After review of the proposed changes, it was determined that the changes will not affect achieving the desired objectives of the F-3 experiment and thus were approved by the GCFR Project. The main result of the changes is that the unsupported length of the fuel rods inside the capsules increases from ~19 in. to ~36 in., but since the fuel rod can only bow 0.011 in. independent of the capsule, this change was accepted. Also, the EBR-II Project now requires all fueled experiments to be xenon tagged. The F-3 fuel-rod capsule drawings have been revised to incorporate the above changes. Some other changes proposed by the GCFR Project, such as the length and location of the charcoal traps, are being incorporated at the same time.

A calculation was performed to determine the axial temperature gradient in the lower axial blanket region of the F-3 experiment fuel rods. The result is shown in Fig. 5.6.

The HECTIC II code[4] received from EBR-II has been made operational on the GGA computer. Some subroutine deletions were necessary because of the size of the program and the storage requirements for the data. The GGA version calculates conditions for all 19 rods of the MK JA assembly at one time and this modified HECTIC code is currently being used to determine temperature distributions in the joint GGA-ANL experiment. Results

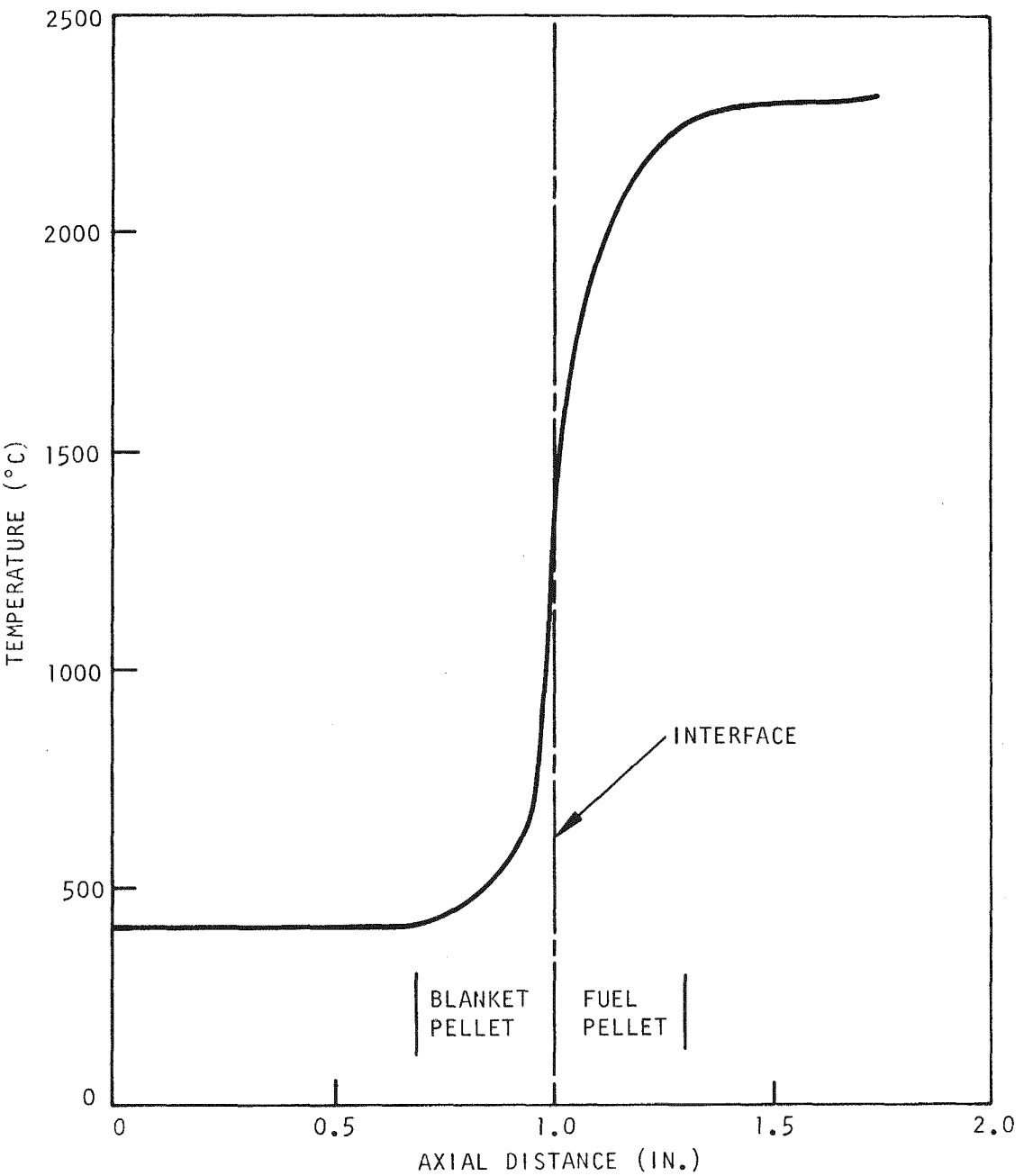

Fig. 5.6 F-3 axial fuel-rod temperatures at the fuel-blanket interface at lower end of the fuel rod with 12.5 kW/ft peak heat generation rate

of the calculations indicated that the outer row of capsules would have had unacceptably large radial temperature gradients of around 60°C due to overcooling in the outer channels; however, the insertion of a shaped filler piece of 0.10 $in.^2$ in cross-sectional area reduces the maximum temperature gradient to 38°C. The temperatures at the various F-3 rod positions are shown in Fig. 5.7. The approval for the Group 08 experiment stipulates that fuel-rod capsules with a coolant flow-through design be employed. This factor may reduce the temperature gradients to even more acceptable levels, but the calculations on the effect of flow through capsules has not yet been made. The location of the capsules in the subassembly is being reexamined to determine if shifts of positions of some fuel-rod capsules will allow the three operating temperatures goals (ANL, <700°C; GGA, 700°C and 750°C) to be more closely approached. The results of a calculation using the HECTIC code by the EBR-II Project was received and when the same input was used at GGA the results were in good agreement, indicating that the accuracy of the two calculations was satisfactory.

The currently planned fuel loadings and conditions for the F-3 experiment are given in Table 5.2.

The F-3 experiment will contain three different fuel rod designs, as shown in Fig. 5.8. The designs differ only in the type and position of the bottom trap and dosimeter assemblies with relation to the bottom blanket pellets. The different axial positions will allow evaluation of activated charcoal trap behavior as a function of fluence since the EBR-II flux falls off rapidly in the axial direction below (and above) the core. Additionally, in the design indicated as Rod 1 in Fig. 5.8, the activated charcoal trap is located just one blanket pellet length away from the fuel. The single blanket pellet separating the fuel from the trap has four axial holes to allow more direct communication between the fission products and the trap than in the other two designs. The capsule design is shown in Fig. 5.9.

The fuel for the F-3 experiment is expected to be delivered to ANL about mid-December 1972.

Table 5.2

F-3 FAST-FLUX IRRADIATION CAPSULE EXPERIMENT

Fuel-rod Capsule Number	Cladding Temperature Calculated (°C)	F-3 Irradiation Conditions						Remarks
		Fuel O/M Ratio	Fuel Density (% TD)	Pellet Geometry	Burnup (MWd/Te) 50,000	Burnup (MWd/Te) 100,000	Charcoal Trap Type	
G-14	676	1.94	88	Solid	—		Active	Initial subassembly loading
G-15	685	1.94	88	Solid	—	—	Active	
G-16	688	1.94	88	Solid	—	—	Sealed	Transient test rod
G-17	690	1.98	88	Solid	—	—	Active	Transient test rod
G-18	689	1.98	88	Solid	—	—	Sealed	
G-19	749	1.94	92	Annular	—		Active	
G-20	749	1.98	92	Annular	—		Active	
G-21	728	1.94	92	Annular	—	—	Active	
G-22	743	1.94	88	Solid	—	—	Active	
G-23	743	1.98	88	Solid	—	—	Active	
G-24[a]	676	1.94	88	Solid		—	Active	Charcoal trap between blanket pellets 1 and 2
G-25[a]	749	1.94	88	Solid		—	Active	
G-26[a]	749	1.94	88	Solid		—	Sealed	

Notes:

All capsules to be gamma scanned and neutron radiographed at 50,000 MWd/Te and 75,000 MWd/Te.

All rods will have a 10-in. fuel column length and will be designed to operate at a nominal maximum heat generation rating of 12.5 kW/ft and 15 kW/ft.

All rods will contain $U_{0.8}Pu_{0.2-x}$ fuel, x = 0.02 or 0.06. At 100,000 MWd/Te burnup, the fluence will be ~1.3×10^{23} n/cm^2.

All rods will have roughened cladding; smear density = 80% to 85% on all rods.

[a]Replacements to be installed at 50,000 MWd/Te exposure.

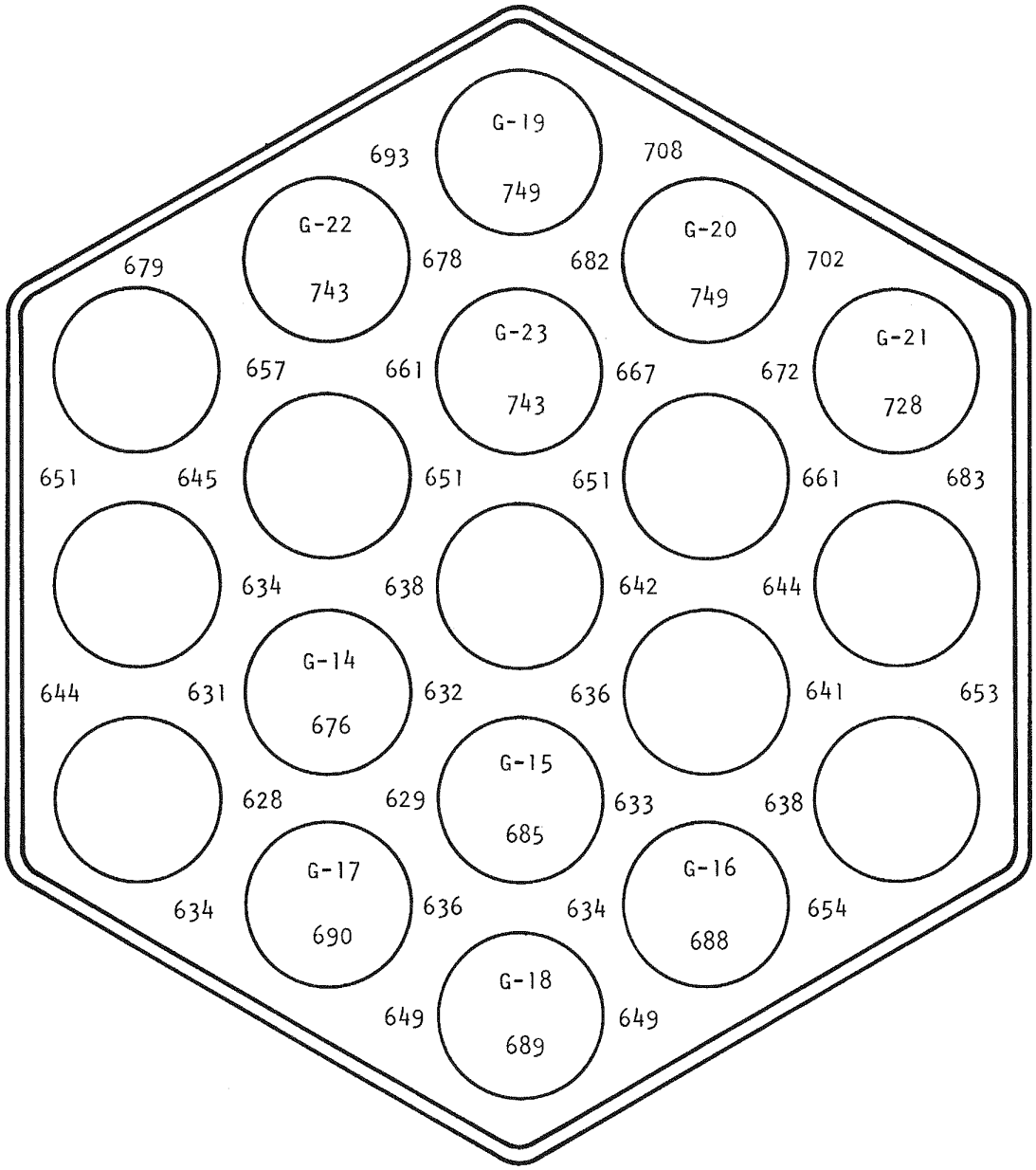

Fig. 5.7 Coolant channel and fuel-rod cladding average OD temperatures (°C) at axial position for maximum temperatures for fuel rods G-14 through G-23 in F-3 fast flux experiment

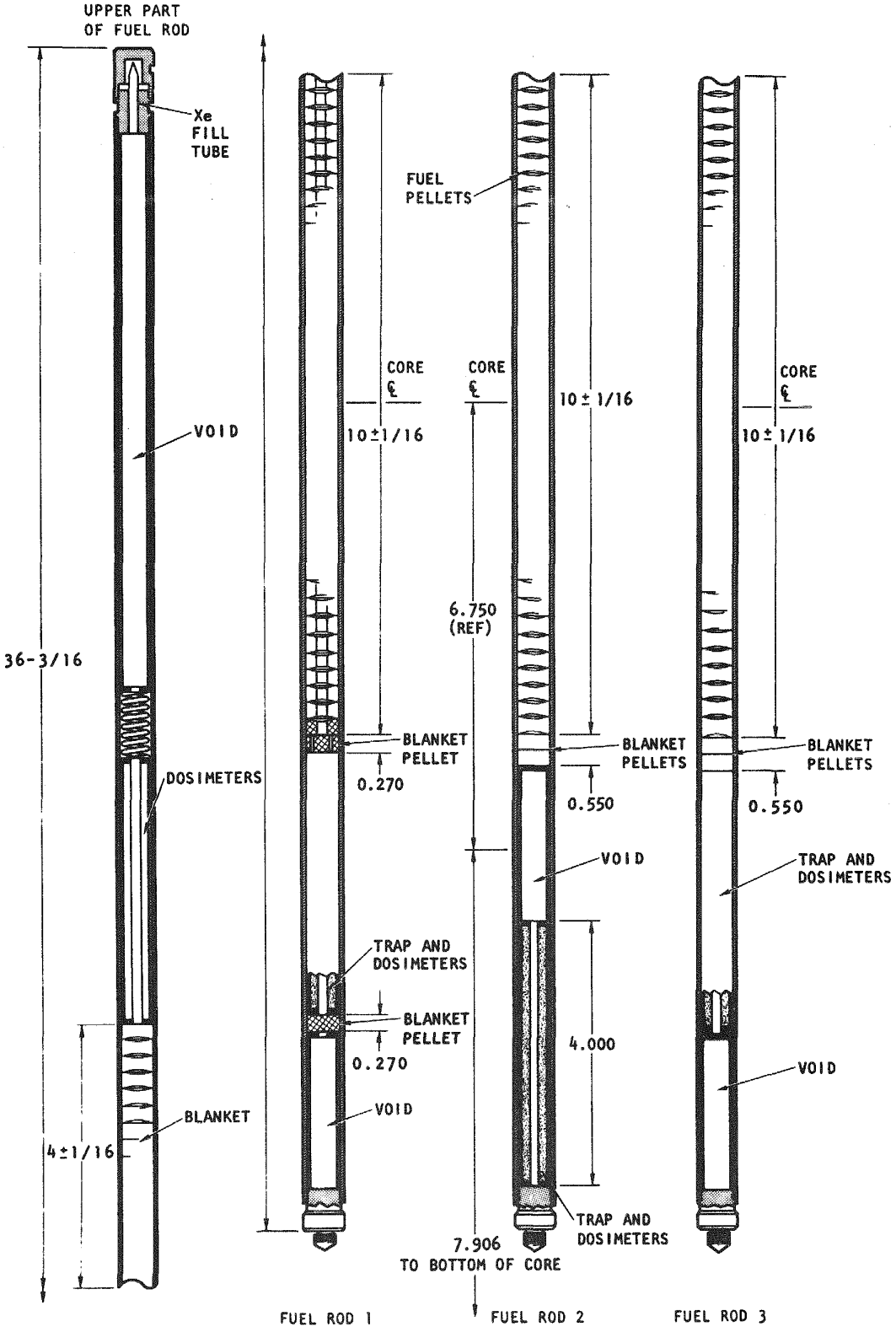

Fig. 5.8 Fuel-rod designs for the F-3 experiment

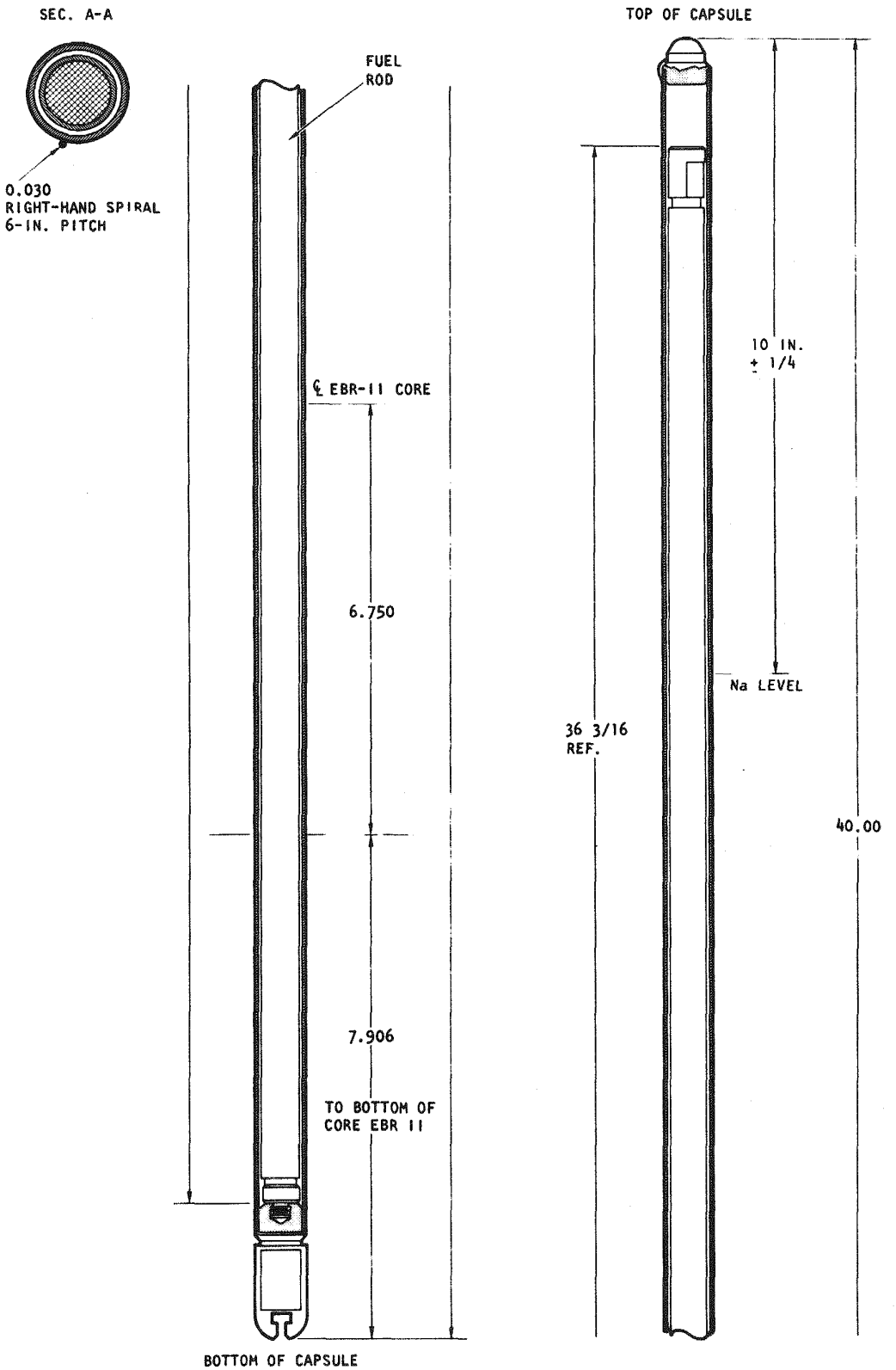

Fig. 5.9 Capsule design for the F-3 experiment

REFERENCES

1. "Gas-Cooled Fast Breeder Reactor Quarterly Progress Report for the Period May 1, 1972 through July 31, 1972," USAEC, Report GA-A12252, Gulf General Atomic, August 31, 1972.

2. Lindgren, J. R., et al., "Planned Thermal Irradiation of Manifolded-Vented $(U,Pu)O_2$-fueled Rod in ORR Capsule P-9," USAEC, Report GA-9896, Gulf General Atomic, March 15, 1970.

3. Vanslager, F. E., "RAD2, A Computer Program for Calculating Fission-product Radioactivities," USAEC, Report GAMD-6519, General Dynamics Corporation, General Atomic Division, July 23, 1965.

4. "HECTIC-II, An IBM-7090 Fortran Computer Program for Heat-transfer Analysis of Gas- or Liquid-cooled Reactor Passages," USAEC, Report IDO-28595 Rev., December 1965.

6. TASK 4700—NUCLEAR ANALYSIS AND REACTOR PHYSICS

Efforts continued on surveillance of LMFBR critical assembly experiments with the objective of establishing an experimentally verified basis for GCFR reactor physics work. Emphasis was placed on calculation of small-sample central worths in the voided inner core of ZPPR-2. Application of two-dimensional transport theory to correct for flux depression in r-z perturbation calculations showed significant improvement in the agreement between measured and calculated worths. Conversion of GGA data files to ENDF/B Version III was completed. Liaison with ANL continued, both through the Industrial Participation Program and through direct contact with members of the ANL staff.

6.1. CRITICAL ASSEMBLY ANALYSIS

6.1.1. Small-sample Central Worth

The small-sample central worth is a simple and basic reactivity measurement consisting of the introduction of a small sample of material at the center of a critical assembly and the recording of the reactivity effect induced by the sample. The central-worth reactivity is calculated with either of two methods: perturbation theory or eigenvalue difference calculations. These measurements and corresponding calculations have been made on a variety of assemblies and for a variety of samples. An apparent discrepancy has persisted in which the calculated worths are systematically higher than the measured worths by a factor ranging from 1.10 to 1.30 and in some cases even higher.

A study is now under way at the Argonne National Laboratory to collect, summarize, and correlate the reported central-worth discrepancies.[1] Davey[2] has recently reported these discrepancies as applied to the ZPPR-2 unvoided cores using ENDF/B Version I data. The calculations reported here are for

the ZPPR-2 voided-inner-core experiments and utilize ENDF/B Version II, which was modified at GGA (see Section 6.5).

The objectives of the central-worth analysis for the voided inner core of ZPPR-2 can be summarized as follows:

1. Test nuclear data used in GCFR nuclear analysis.
2. Determine the adequacy of various calculational models by comparing the calculations with measurements.
3. Develop expertise in critical assembly analysis.
4. Provide independent calculations for comparison with calculations being performed by LMFBR analysts.

These objectives apply to all calculations performed under the GGA surveillance program of the LMFBR critical assembly work.

6.1.1.1. Calculation of Small Central Worths in ZPPR-2. The calculational program began with a series of one-dimensional diffusion theory eigenvalue difference calculations.[3] The methodology has been extended to r-z perturbation theory with a two-dimensional transport calculation of the flux depression factor. These methods are discussed below. The results of the calculations to date of the central worths in the voided inner core of ZPPR-2 are summarized in Tables 6.1 and 6.2. All of the calculations are listed in Table 6.1, and the specific results for each sample using r-z perturbation theory are given in Table 6.2.

One-dimensional Diffusion Theory Calculations. The results of these calculations were reported in the previous quarterly report.[3] The adequacy of this method depends on the extent to which the assembly (in this case ZPPR-2) can be represented as a spherical assembly. The results to date indicate that spherical geometry does not adequately describe ZPPR-2.

One-dimensional Transport Calculation. The first refinement in the methodology was the use of a one-dimensional transport calculation. The code employed was 1DFX[4] using 10 groups, S_8 angular quadrature, and spherical geometry. Acknowledging the inadequacy of spherical geometry for ZPPR-2, a significant improvement was obtained for the boron sample in which the calculated to experimental discrepancy (C/E) decreased from 1.61

Table 6.1

COMPARISON OF CALCULATIONAL METHODS FOR THE ANALYSIS OF SMALL-SAMPLE WORTHS IN ZPPR-2 WITH VOIDED INNER CORE

Parameters	Diffusion Theory (1-D)	Transport Theory (1-D)	R-Z Perturbation Theory		
			Unshielded	1DFX Shielding	DOT Shielding
Geometry	Spherical	Spherical	Cylindrical	Cylindrical	Cylindrical
Number of groups	27	10	10	10	10
Sample worth	Δk	Δk	Perturbation	Perturbation	Perturbation
Sample geometry	Infinite dilute	Equal volume	Cylindrical	Cylindrical	Cylindrical
Flux depression	None	----	None	1-D transport	2-D transport
Average (C/E)	1.38	----	1.20	----	----
B-10 sample C/E	1.61	1.26	1.35	0.855	1.19

Table 6.2

COMPARISON OF CALCULATED AND EXPERIMENTAL VALUES FOR ZPPR-2 CORES

Material	C or E	Unvoided 93-drawer Plate Zone ANL Calculated[a]	Voided	
			93-drawer Plate Zone GGA Calculated[b]	69-drawer Pin Zone GGA Calculated
B-1 (boron)	C	-2583.4	-1780	
	E	-2286.6	-1314	
	C/E	1.13	1.35	
Fe-1 (iron)	C	-3.60	-3.15	
	E	-3.06	-3.55	
	C/E	1.18	0.886	
U-6 (93% U^{235})	C	114.7	99.2	
	E	96.0	81.6	
	C/E	1.195	1.22	
DU-6 (depleted U)	C	-9.43	-7.38	
	E	-6.63	-6.01	
	C/E	1.42	1.23	
Pu-30 (Pu^{239})	C	134.98	130.8	138.0
	E	117.39	117.6	115.0
	C/E	1.15	1.11	1.20
Pu-48	C		85.35	
	E		73.69	
	C/E		1.16	
C-1 (carbon)	C		-20.82	-15.31
	E		-17.51	-14.34
	C/E		1.19	1.07

[a] From Ref. 2.

[b] R-z perturbation calculations with no flux depression factors.

using diffusion theory to 1.26 using transport theory. The improved agreement is due to the ability of the transport code to more adequately treat the flux depression in the sample. However, this depression may be overemphasized in spherical geometry.

Two-dimensional R-Z Perturbation Calculations. In order to avoid the uncertainties associated with applying one-dimensional methods to ZPPR-2, a series of two-dimensional perturbation calculations were made for the Doppler and small-sample central worths for the voided inner core of ZPPR-2.

Perturbation theory assumes that the flux in the system is not perturbed by the sample. Worths are calculated utilizing unperturbed regular and adjoint fluxes. For absorbing materials such as boron and depleted uranium, a correction must be applied to account for the flux depression in the sample. A second-order correction should also be applied for flux depression in the region outside the sample.

The sensitivity of the boron worth to the flux depression factor was calculated. The flux depression factor for each group, DF_g, is defined as

$$DF_g = \left(\frac{\bar{\phi}_S}{\phi_0}\right)_g \left(\frac{\bar{\phi}^*_S}{\phi^*_0}\right)_g \tag{6.1}$$

where $\bar{\phi}_S$ and $\bar{\phi}^*_S$ are the average fluxes (regular and adjoint, respectively) in the sample and ϕ_0 and ϕ^*_0 are unperturbed average fluxes (regular and adjoint, respectively).

The regular and adjoint fluxes $\bar{\phi}_S$ and $\bar{\phi}^*_S$ were obtained from an 1DFX transport calculation using 10 groups, S_8 quadrature, and spherical geometry. It was concluded that approximating Eq. (6.1) by

$$DF_g = \left(\frac{\bar{\phi}_S}{\phi_0}\right)_g \tag{6.2}$$

results in a depression factor that is within 10% of the exact value. Since the flux depression factor is approximately 30% for the boron sample, the overall error in assuming the flux is self-adjoint is approximately 3%. The results of applying the exact formulation to the boron sample is shown in Table 6.1, where the C/E improved from 1.35 to 0.855.

Since the sample geometry is cylindrical, not spherical, the flux depression factor is probably overestimated. This was checked by calculating the flux depression utilizing the two-dimensional transport code DOT.[5] A top and right isotopic surface source was incident on the boron sample; an S_8 quadrature, 10 groups, and 100 mesh intervals were used. Applying the DOT calculated flux depression factor improved the C/E ratio from 1.35 to 1.19.

6.1.1.2. Conclusions of Study to Date. From the studies to date, the following conclusions can be drawn:

1. One-dimensional diffusion theory is inadequate for ZPPR-2.
2. One-dimensional transport theory appears to improve the C/E ratio; however, for highly absorbing cylindrical samples, spherical transport theory may lead to fortuitous results because the absorption rate in the sample is overpredicted.
3. R-z perturbation theory appears to be adequate provided the flux depression is properly treated.
4. ENDF/B Version II (modified) appears to be adequate for materials studied to date.

6.1.2. Calculation of Doppler Worth in the Voided Inner Core of ZPPR-2

The Doppler worth of a small UO_2 sample was calculated using r-z perturbation theory. Since the cross sections in the GGA data file are presently available at 300°K and 1300°K, the ANL experimental values at 500°, 800°, and 1100°K were linearly extrapolated out to 1300°K; the extrapolation is shown in Fig. 6.1. The extrapolated measured value at 1300°K is 0.50 Ih/kg, which agrees quite well with the calculated value of 0.535 Ih/kg, resulting in a C/E = 1.07. No flux depression factor has been applied, but it is estimated to be approximately 5 to 10%.[6] Calculations of the flux depression factor using the DOT code are planned.

6.1.3. β_{eff} and Prompt Lifetime Calculations for ZPPR-2

The effective delayed neutron fraction, β_{eff}, for ZPPR-2 has been calculated with the GGA r-z perturbation code. The prompt neutron lifetime, ℓ,

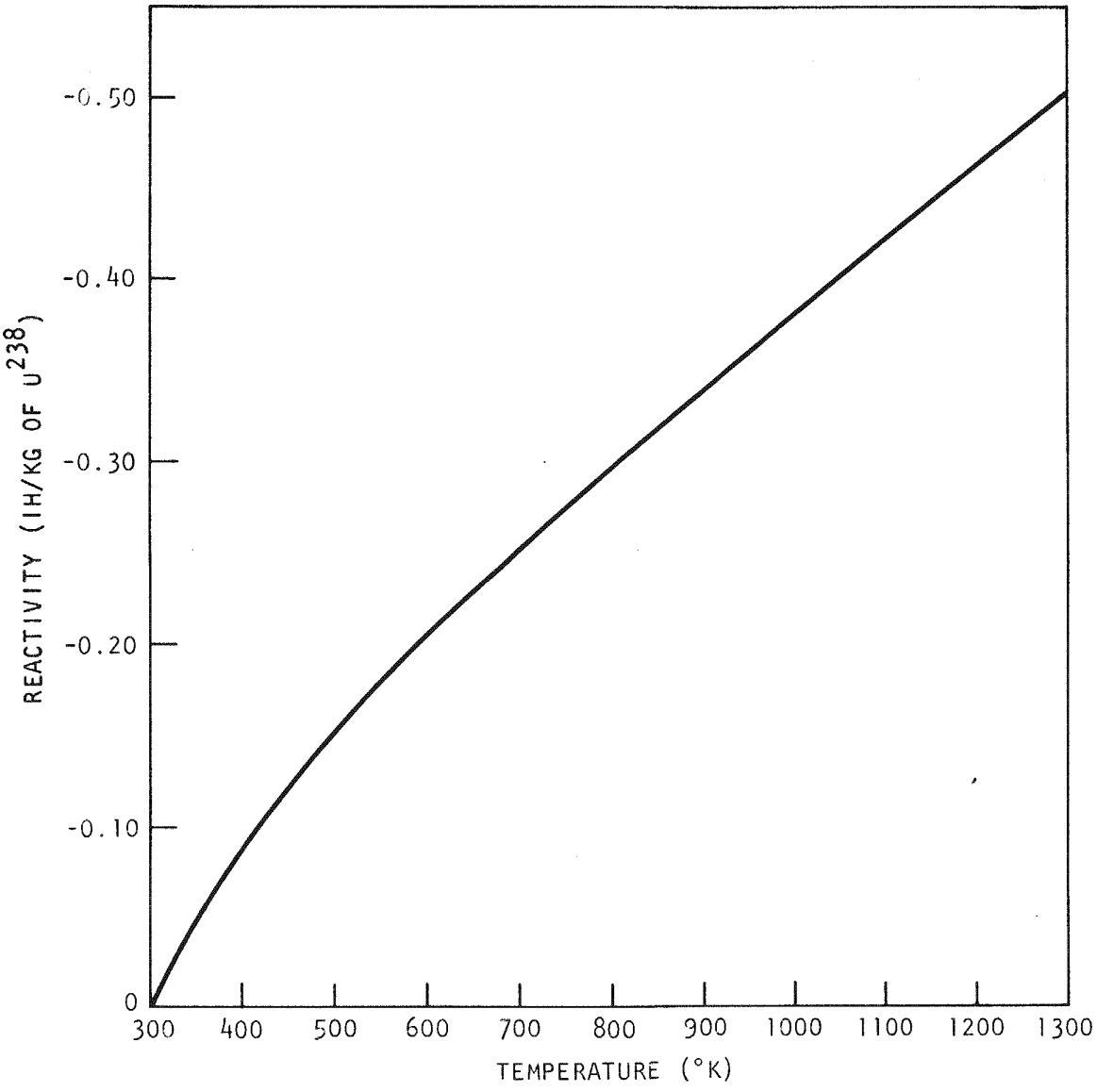

Fig. 6.1 Extrapolated Doppler worth of UO_2 sample in 69-pin voided zone of ZPPR-2

was also calculated. The results are in good agreement with those obtained by ANL:

	GGA	ANL[a]
β_{eff}	0.003232	0.003180
ℓ, sec	5.20×10^{-7}	5.58×10^{-7}

[a]See Ref. 7.

6.2. ANL LIAISON

Liaison was increased at the working level this past quarter. Several meetings were held with the Argonne staff both at Argonne and at the American Nuclear Society National Topical Meeting on New Developments in Reactor Physics and Shielding. Discussions centered on GGA analysis of LMFBR critical assembly experiments and planning of experiments specifically designed to test GCFR design methods and data.

6.3. GCFR CROSS SECTIONS

Conversion of the GGA data files for GCFR to ENDF/B Version III has been completed. Sensitivity studies are planned for the next quarter. A comparison was made between the GGA data files for U^{238} and Pu^{239}, which are based on a modified[8] ENDF/B Version II set.

The GGA ENDF/B Version II (modified)[8] capture cross sections for U^{238} are compared in Fig. 6.2 to those obtained with ENDF/B Version III, obtained from Ref. 9. The GGA ENDF/B Version II (modified) data closely matches the evaluation, and thus no change is expected with regard to U^{238} in going from ENDF/B Version II (modified) to ENDF/B Version III.

Pu^{239} alpha (σ_c/σ_f) obtained from two data sets, namely, an ANL 27-group set[10] based on ENDF/B Version III and the GGA 23-group set based on ENDF/B Version II (modified)[8] are compared in Fig. 6.3. Again, there is only a slight difference in the alpha values obtained with ENDF/B Version III from those of the GGA data files.

It can therefore be concluded that for the two important isotopes U^{238} and Pu^{239}, little difference can be expected in coverting from ENDF/B Version II (modified) to ENDF/B Version III.

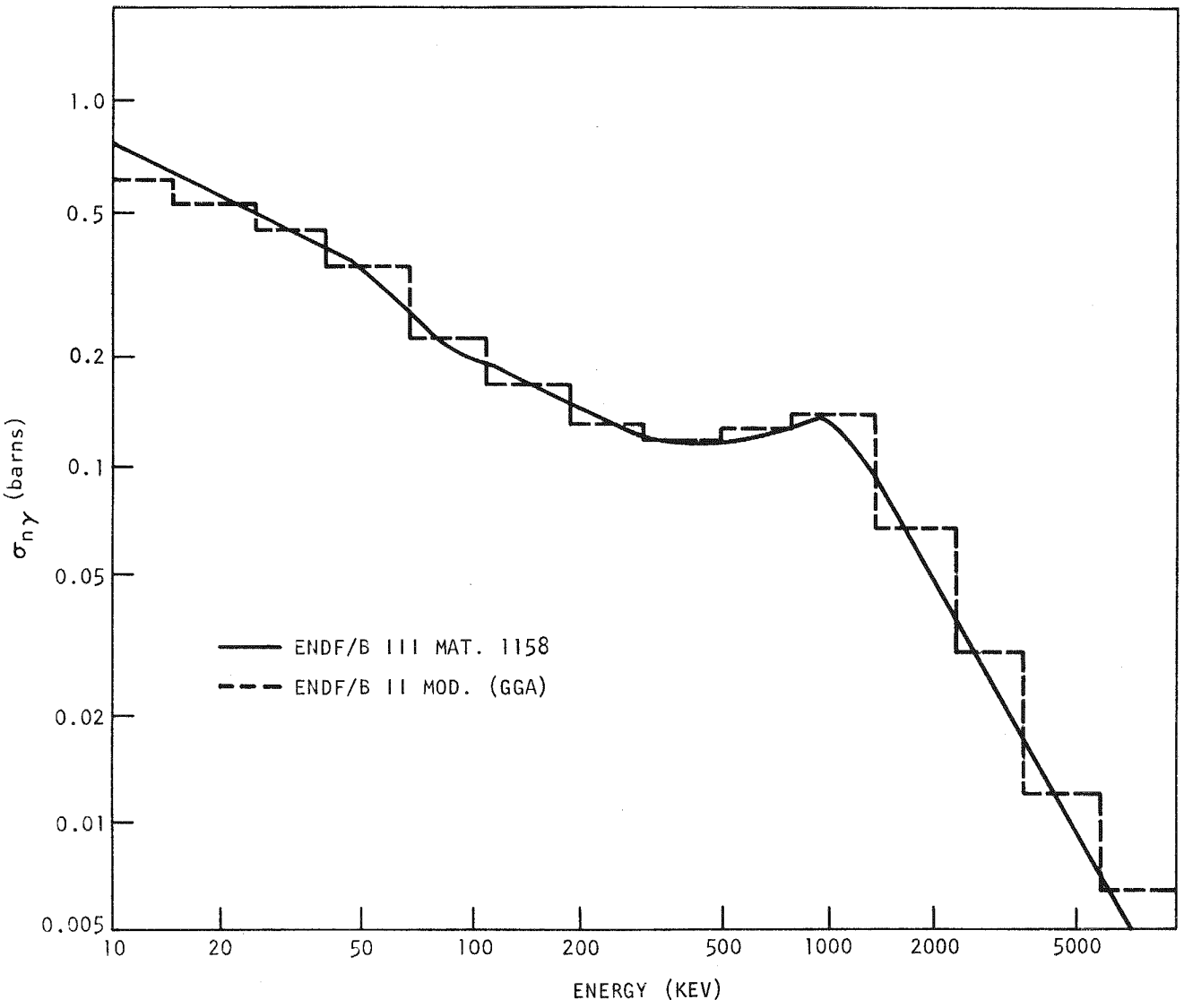

Fig. 6.2 Comparison of ENDF/B III with GGA ENDF/B II (modified)

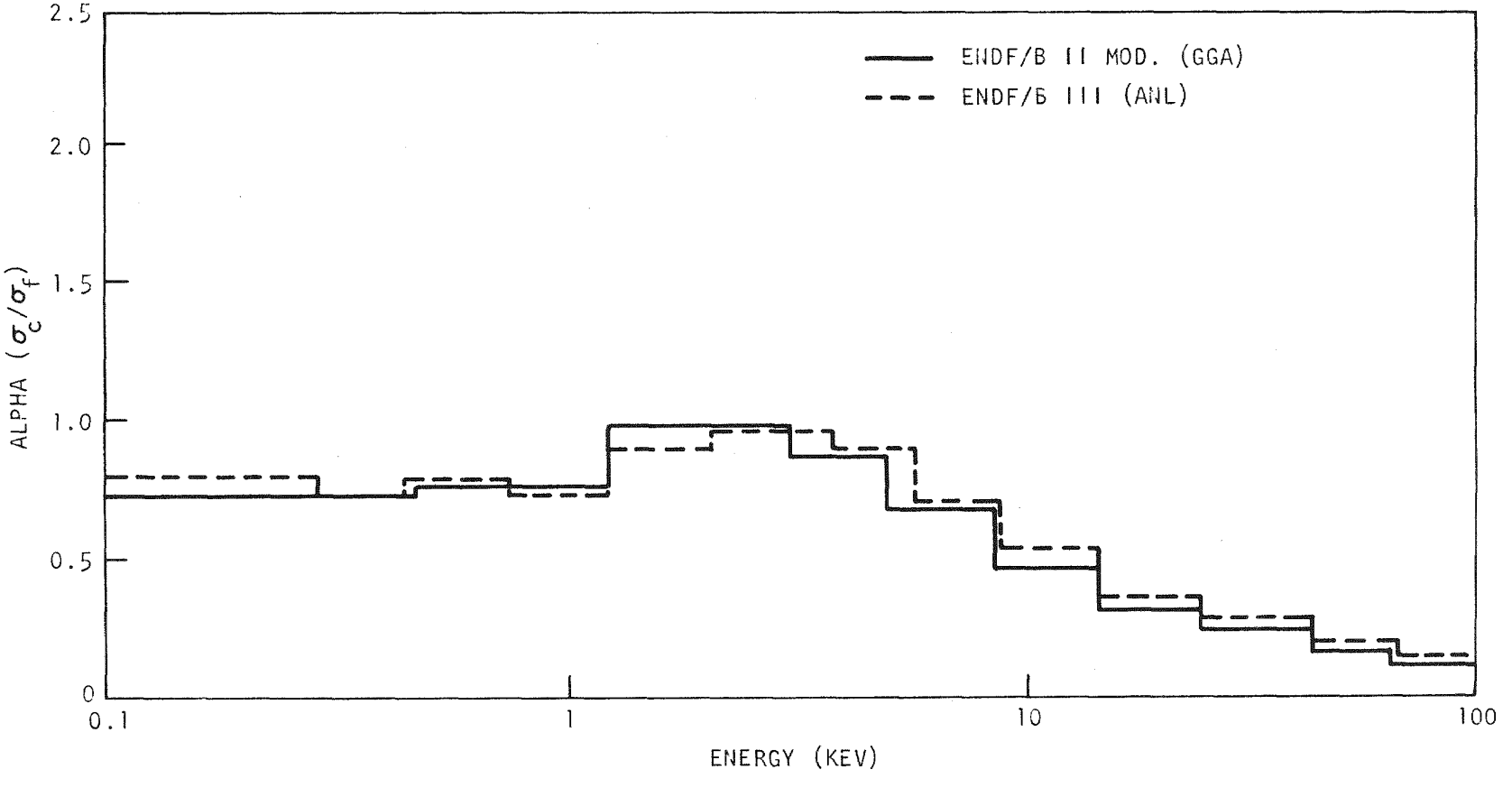

Fig. 6.3 Comparison of GGA ENDF/B II (modified) and ANL ENDF/B III calculated alpha for Pu^{239}

REFERENCES

1. Bohn, E. M., Applied Physics Division, Argonne National Laboratory (private communication).

2. Davey, W. G., "The Demonstration Benchmark Program," Proceedings of the ANS National Topical on New Developments in Reactor Physics and Shielding, USAEC, Report TID-4500, September 1972.

3. "Gas-Cooled Fast Breeder Reactor Quarterly Progress Report for the Period May 1, 1972 through July 31, 1972," USAEC, Report GA-A12252, Gulf General Atomic, August 31, 1972.

4. Lathrop, K. D., "DTF-IV, A Fortran-IV Program for Solving the Multigroup Transport Equation with Anisotropic Scattering," USAEC, Report LA-3373, Los Alamos Scientific Laboratory, November 1965.

5. Mynatt, F. R., "DOT, Two-Dimensional Discrete Ordinates Transport Code," CCC-89-1C-1694 RSIC-ORNL (1969).

6. Till, C. E., Applied Physics Division, Argonne National Laboratory (private communication).

7. Kaiser, R. E., et al., Argonne National Laboratory (private communication).

8. Pellaud, Bruno, "The Physics Design of the Gas-Cooled Fast Reactor Demonstration Plant," USAEC, Report GA-10509, Gulf General Atomic, August 29, 1971.

9. Drake, M. K., "The Basis of Current Evaluated Data Files," Proceedings of the ANS National Topical on New Developments in Reactor Physics and Shielding, USAEC, Report TID-4500, September 1972.

10. Zolotar, B. A., Applied Physics Division, Argonne National Laboratory (private communication).

Appendix

PUBLICATIONS

"Planned Thermal Irradiation of Manifolded-Vented (U, Pu)O_2-fueled Rod in ORR Capsule GB-10," by J. R. Lindgren, et al., USAEC, Report GA-A12123, July 31, 1972.